Portable Device for Operating Graphene Ion Sensitive Field Effect Transistors

Raed Abdo

Department of Electrical and Computer Engineering

McGill University

Montreal, Quebec, Canada

August 2020

Under the supervision of Professor Thomas Szkopek

A thesis submitted to McGill University in partial fulfillment of the requirements

for the degree of Master of Engineering.

Abstract

In this thesis, we present large-area graphene-based ion sensitive field effect transistor (ISFET) as an attractive candidate for detecting ion concentrations in a solution on-site using a portable device. Graphene ISFETs are compact and low-cost sensors that can be used in real-time and on-site. They also offer a resolution that is comparable to a spectrophotometer and atomic absorption spectrometer (AAS), which are high cost, bench-top laboratory instruments ill-suited for on-site measurements. We have been using a semiconductor parameter analyzer (SPA) to operate graphene ISFETs but they share the same limitations as high cost, bench-top laboratory instruments. We used an SPA because it is a low noise device where the inherent noise that is introduced in our measurements is predominantly from the graphene ISFETs.

We present here a portable device that we designed and built as on-site alternative to the SPA. We discuss the design and development process of the portable device to fulfill the same functionality as the SPA. Mainly, the portable device's interrogation circuit biases a graphene ISFET and measures the drain-source current (I_{ds}) that correlates to a molar concentration of an ion in an analyte. The portable device has a customized case that holds a graphene ISFET and the interrogation circuit. Additionally, the portable device is connected to an Internet of things (IoT) platform that enables real-time access to measurements. The interrogation circuit is powered by a pocket size 24 Ah battery bank that can provided more than 40 hours of continuous use.

We calibrated three graphene ISFETs, correlating the molar concentration to the I_{ds} of each graphene ISFET designed for detecting K^+, $Na^{+,}$ and NH_4^+ ions in a solution, using the SPA and the portable device. We compared the graphene ISFET performance as interrogated by the SPA and the portable device in terms of resolution (R), detection limit (D), sensitivity (S), and I_{ds} root mean

square (RMS) fluctuation (ΔI_{ds}). The detection limit (D) and sensitivity (S) were comparable between the portable device and the SPA, to within the limits imposed by drift in sensor performance between measurements conducted in this study. The fluctuation in current (ΔI_{ds}) and thus the resolution (R) was at most three times larger for graphene ISFETs interrogated with the portable device as compared to the SPA. Lastly, we present an example of on-site and real-time measurements using the portable device.

Abrégé

Dans cette thèse, nous présentons un transistor à effet de champs sensible aux ions (ISFET) fait à partir de graphène de grande surface comme candidat pour détecter des concentrations d'ions dans une solution sur-site, grâce à un dispositif portatif. Les ISFETs de graphène sont des détecteurs compacts et non-dispendieux, qui peuvent être utilisés en temps réel sur-site. Ceux-ci offrent une résolution comparable à celle d'un spectrophotomètre ou d'un spectromètre à absorption atomique (AAS), qui sont dispendieux, conçus pour le laboratoire et ne sont donc pas des instruments utilisables pour des prises de mesures sur-site. Nous avons employé un analyseur de paramètres semiconducteurs (SPA) afin de mettre en opération les ISFETs de graphène, malgré que ceci souffre des mêmes limitations que les instruments de mesures dispendieux uniquement conçu pour le laboratoire. Le SPA a été utilisé pour son faible bruit lors des mesures, là où le bruit intrinsèque introduit dans les mesures provient particulièrement des ISFETs de graphène.

Nous présentons ici un dispositif portatif que nous avons conçu et fabriqué comme alternatif au SPA. Nous discutons alors de sa conception et du processus de développement afin d'obtenir une fonctionnalité identique au SPA. Principalement, le circuit d'interrogation du dispositif introduit un biais dans un ISFET de graphène et mesure le courant source-drain (I_{ds}) qui est corrélé avec la concentration molaire d'un ion dans un analyte. Le dispositif portatif est composé d'un étui personnalisé qui contient le ISFET de graphène ainsi que le circuit d'interrogation. De plus, le dispositif portatif est connecté auprès d'une plateforme d'internet des objets (IoT) qui permet

l'accès aux mesures prises en temps réel. Le circuit d'interrogation est alimenté d'une pile de 24Ah portatif, capable de fournir plus de 40 heures d'utilisation continue.

Nous avons calibré trois ISFETs de graphène, en corrélant la concentration molaire avec le I_{ds} de chaque ISFET fabriqué pour détecter le K^+, le Na^+ et le NH_4^+ en solution, avec le SPA et le dispositif portatif. Nous avons comparé la performance du ISFET de graphène interrogé par le SPA et le dispositif portatif en termes de la résolution (R), la limite de détection (D), la sensibilité (S) et la valeur moyenne quadratique (RMS) des fluctuations de I_{ds} (ΔI_{ds}). La limite de détection et la sensibilité étaient comparables entre le dispositif portatif et le SPA, à l'intérieur des limites définies par la dérive de la performance de détecteurs entre les mesures de cette étude. La fluctuation du courant ΔI_{ds} et ainsi la résolution était en dessous de trois fois plus pour les ISFETs de graphène interrogés avec le dispositif portatif que pour le SPA. Finalement, nous présentons un exemple de prise de mesures sur-site en temps réel avec le dispositif portatif.

Acknowledgements

First and foremost, I would like to thank my supervisor, Professor Thomas Szkopek, for providing me with the opportunity to work in his lab. His mentorship and guidance have enhanced my integrity, my ability to solve problems systematically and methodically, and communicate my approach and findings in a coherent manner. I would particularly like to thank him for his patience in helping me overcome learning hurdles that were hindering me from reaching my potential. The impact he has made on me exceeds research and academia.

I would like to thank Ibrahim Fakih for making the graphene ISFETs. This project would have not been possible without the stride he has made in bringing the ISFETs operations to a reliable capacity. I also want to thank him for supporting me and collaborating with me during the development process of the portable device to ensure optimal functionality of the portable device for the ISFETs. I also want to thank all my current and past colleagues for creating an inclusive environment the empowered me to overcome many of the challenges that I faced.

I want to thank the Natural Sciences and Engineering Research Council of Canada, and in particular the NSERC- Green Electronics Network (NSERC-GreEN) for funding the project. I also want to thank them for their generous stipend that allowed me to focus on my research and not worry about acquiring funding from external sources. I would also like to thank McGill Dobson Centre for Entrepreneurship for funding us to spin off a startup from this technology.

Finally, I would like to thank my parents for their unconditional level and support. I dedicate this thesis to them and to the parents of researchers who spend their lives in the pursuit of knowledge.

Contents

List of Tables

List of Figures

Abbreviations

AAS	absorption spectrometer
ADC	analog to digital converter
D	detection limit
DAC	digital to analog converter
DI	de-ionized
DIP	dual in-line package
EPA	Environmental Protection Agency
FET	field effect transistor
IC	integrated circuit
IoT	internet of things
ISE	ion sensitive electrode
ISFET	ion sensitive field effect transistor
M	molar concentration
MOSFET	metal-oxide semiconductor field-effect transistor
OPA	operational amplifier
OS	operating system
PCB	printed circuit board
R	resolution
RMS	root mean squared
S	sensitivity

SBC	single board computer
SMU	source measurement unit
SPA	semiconductor parameter analyzer
WHO	World Health Organization

Symbols

a	ion concentration in Bergveld model
A	transistor channel area
α	ISFET sensitivity factor, dimensionless number between 0 and 1
C	capacitance per unit area between the channel and electrolyte
C_i	Transistor gate oxide capacitance per unit area
C_{final}	solution final molar concentration
$C_{initial}$	solution initial molar concentration
Δf	bandwidth of the electrical measurement circuit
ΔI_{ds}	transistor drain-source channel current RMS fluctuation
ΔV	voltage RMS fluctuation
ΔV_{out}	output voltage of transimpedance amplifier fluctuation measured by the ADC
e	electron charge
f	frequency
g_m	FET transconductance
i_n	current noise
i_s	signal current
i_x	current noise power
I_{triode}	current in the triode region
I_{ds}	transistor drain-source channel current

$I_{ds\text{-}max}$	transistor maximum drain-source channel current
$I_{ds\text{-}min}$	transistor minimum drain-source channel current
$I_{ds\text{-}range}$	transistor drain-source channel current range for a molar concentration range
k_B	Boltzmann's constant
L	transistor channel length
N_0	areal density of active sites in the sensitive layer contributing to chargefluctuation
μ	transistor charge carrier effective mobility
R_{in}	input resistance
R_f	feedback resistance
R_V	voltage resolution of the device, smallest measurable change of voltage.
T	absolute temperature in Bergveld model
V_{ds}	transistor drain source voltage
V_{np}	transistor gate voltage where minimum point of conduction, neutrality point, occurs
V_{out}	output voltage of transimpedance amplifier
V_s	transistor voltage at the source terminal
V_d	transistor drain voltage
V_G	transistor gate voltage
V_{final}	solution final volume
V_{final}	solution initial volume

V_{ref}	transistor reference voltage
V_T	transistor threshold voltage
W	transistor channel width
ψ_0	surface potential at the sensing layer/electrolyte interface

1. Introduction

1.1 Current Methods for Measuring Ion concentration

The measurement of ion concentration accurately, in real-time, and on-site is essential in a vast range of applications that include, water quality monitoring [1], wastewater treatment [2], food processing [3], pharmaceutical production [4], and clinical applications [5]. There are several ways to measure the ion concentration in water accurately, the main ones are; 1. spectrophotometry, 2. atomic absorption spectroscopy, and 3. potentiometry [6], [7], [8]. Spectrophotometry and atomic absorption spectroscopy can measure very low ion concentration in water accurately and precisely [6]. We define a few terms that will be used throughout this paper. Resolution (R) is the smallest measurable change in molar concentration that can be measured. Detection limit (D) is the lowest measurable molar concentration, in other words, the lowest concentration that can be measured. Sensitivity (S) is the change in current or voltage per decade of molar concentration. Real-time measurement is the ability to measure the concentration with negligible time delay. In the context of environmental monitoring applications, the relevant time delay for real-time measurement is a few seconds. The term on-site, refers to the ability to carry out measurements at the site of the water source. For example, a lake, factory, or river. Table 1.1. illustrates a comparison between the different measurement methods in terms of cost, resolution, size, and real-time and on-site measurement for pH.

Measurement method	Cost	Minimum Resolution	Size	Real-time and on-site Measurement
Spectrophotometry	$50k-$100k	~ 0.1 mpH	~ m	No

Potentiometry – Glass Electrode	$500-$2k	~ 5 mpH	~ mm	Yes
Potentiometry – Silicon ISFET	$500-$2k	~ 2 mpH	~ mm	Yes
Potentiometry – Graphene ISFET	<$100	~ 0.1 mpH	~ mm	Yes

Table 1.1: The cost, resolution, size, real-time and on-site measurement for different measurement methods of pH [6], [9], [10], [11], [12].

We can see that spectrophotometry offers the highest resolution of ~ 0.1 mpH. However, both these methods require large and expensive equipment making them an unfeasible option especially for real-time and on-site measurements [6]. Potentiometric sensors are very attractive candidates for real-time and on-site measurements, due to their relatively small size, and potential for real-time, and on-site measurement but they lack in terms of their resolution, except for graphene ion selective field effect transistors (ISFETs) [6] [12]. Graphene ISFETs are low size, low cost, can be used in real-time and on-site and offer a resolution comparable to that of spectrophotometry and atomic absorption spectroscopy [12]. Graphene ISFETs are a type of potentiometric sensors [6]. Potentiometric sensors measure the potential difference between two electrodes [11]. The potential difference is used to infer the concentration of the ion of interest in a solution [10]. Potentiometric sensors are ion selective electrodes (ISE) or silicon based ISFETs [6]. By incorporating graphene into ISFETs, the resolution is enhanced, achieving a resolution of 0.1 mpH for hydrogen [6]. Broadly speaking, a sensitivity (also known as Nernstian response) of 59 mV per decade over the concentration range 10^{-5} to 10^{-1} M for various ion solutions was achieved for several ion sensitive graphene ISFETs [6] [12]. A large and low noise device known as a Semiconductor Parameter Analyzer (SPA) was used to calibrate and test the graphene ISFETs to record the detection limit, resolution, and sensitivity mentioned earlier [6]. Having understood the graphene ISFET's operation, a compact interrogation circuit was

developed to operate the ISFET. In this thesis, we refer to the term *sensor* as the graphene ISFET. We refer to the term *portable device* as the interrogation circuit with its case and the connection to the graphene ISFET. The portable device was developed and tested for three sensors that can detect one of the following ions; K^+, Na^+, or NH_4^+. Finally, the portable device was incorporated into an internet of things (IoT) platform. This allowed us to monitor molar concentration measurements across various geographical locations in real-time. To properly understand how the portable device works we will first need to understand how ISFETs work and what makes graphene ISFETs unique.

1.2 Ion Sensitive Field Effect Transistors (ISFETs)

We briefly review the operating principle of an ISFET, which is important in determining the requirements of the interrogation circuit. ISFETs are one of the most common chemically sensitive field-effect transistors [11]. They were first developed and demonstrated by Bergveld in 1970 [10]. An inclusion of a reference electrode in contact with the electrolyte was later reported in 1974 [10]. The structure of ISFETs are based on those of metal-oxide semiconductor field-effect transistors (MOSFETs) [11]. The fundamental modification is the replacement of a metallic gate with an electrolytic solution [10], [11]**.** Fig. 1.1 illustrates the fundamental structure of an ISFET.

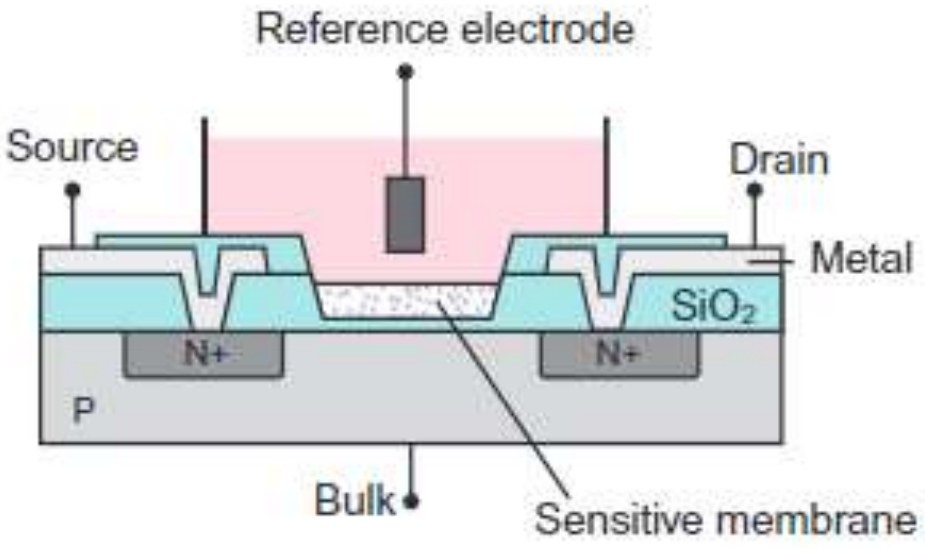

Fig. 1.1: An illustration of the structure of an ISFET [11]**.**

The transistor lays on top of a p-type silicon substrate (an n-type substrate could also be used, with corresponding changes in transistor structure). The source and the drain are separated by a channel with layers of silicon dioxide and a metal gate placed on top in a conventional FET structure. The length and width of the ISFET channel is typically on the order of tens to hundreds of microns [10]. Due to the fundamental requirement of detecting ions, the electrolyte containing the ions is in direct contact with the top layer. In early ISFETs, the conventional poly-Si gate of a MOSFET is replaced with the electrolyte, which functions as the gate [11]. The electrolytic solution is directly in contact with a sensitive layer designed to maximize the sensitivity and selectivity of the ion of interest and prevent the solution from penetrating the surface to reach the SiO_x or Si interface. More complex structures employing back end of line processing of conventional MOSFETs are typically found in modern ISFET implementations. The ion sensitive layer can either be dielectrics such as Al_2O_3, and Ta_2O_5 or plastic membranes infused with

ionophores. A reference electrode, often a Ag/AgCl electrode, is used to regulate the electrolytic potential. The voltage applied to the electrolytic solution acts as the reference voltage, which is equivalent to gate voltage (V_G) of a MOSFET. In the case of a MOSFET, applying a gate voltage above the threshold voltage creates an inversion layer and allows current flow from the source to the drain. The threshold voltage (V_T) is the voltage required to turn the transistor on. The transistor can operate in either the triode region or saturation region, depending on the applied drain voltage (V_D) [10]. The triode region has the following I-V characteristic:

$$I_{Triode} = \frac{\mu C_i W(V_G - V_T)V_D}{L}$$

The saturation region has the following I-V characteristic:

$$I_{Saturation} = \frac{\mu C_i W(V_G - V_T)^2}{2L}$$

where μ is the charge carrier effective mobility, C_i is the gate oxide capacitance per unit area, V_G is the gate voltage, V_T is the threshold voltage, V_D is the drain voltage, W is the gate width, and L is the gate length [10]. Fig. 1.2 illustrates the electric schematic of an ISFET [10].

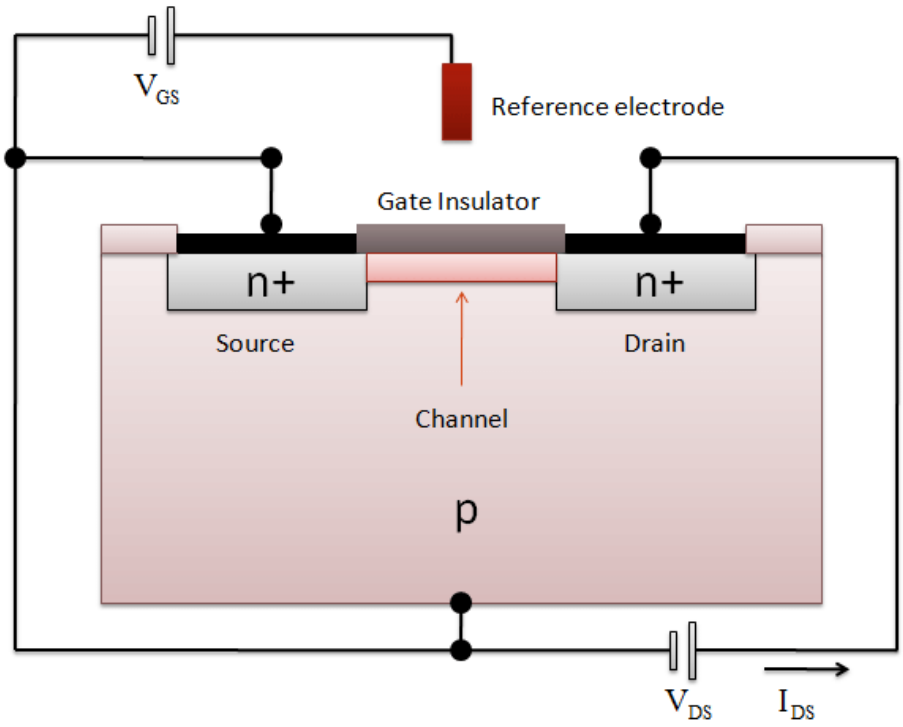

Fig. 1.2: An illustration of the electric schematic of an ISFET [13].

For an ISFET, the same characteristics apply but the threshold voltage has different contributions [6]. The ISFET is sensitive to changes in the ion concentration through the modulation of the surface potential of the insulator (ψ_0) due to a dipole layer at the dielectric side of the electrolyte/dielectric interface with ion concentration [12]. This is described quantitatively with the Bergveld model [12]. The Bergveld model leads to a sensitivity described by the following equation:

$$\frac{\delta\psi_0}{\delta \log|a|} = \alpha \ln 10 \frac{k_B T}{e}$$

where *a* is the ion concentration in question, *e* is the electron charge, k_B is Boltzmann's constant, *T* the absolute temperature, and α is a dimensionless sensitivity factor between 0 and 1 that depends on the properties of the ion sensitive layer and the electrolyte. Ideally, α = 1 and the

ISFET sensitivity is 59.2 mV/ decade at room temperatures. This is known as the Nernstian limit. However, a sub-Nernstian response can arise from non-ideal ion sensitive layers where $\alpha < 1$ [6].

The ISFET's signal current is proportional to molar concentration of the electrolyte [10]. The ISFET's signal current is expressed as follows:

$$\mathrm{i_S} = \mathrm{g_m}\delta\varphi_0$$

where g_m is the (field effect transistor) FET transconductance. The signal to noise ratio (SNR) of the power noise current can be expressed as follows:

$$\mathrm{SNR} = \frac{<\mathrm{i_s^2}>}{<\mathrm{i_n^2}> + <\mathrm{i_x^2}>}$$

where $< i_n^2 >$ is the current noise power from the ISFET and $< i_x^2 >$ is the current noise power from the read-out electronics [6]. ISFET noise is dominated by charge fluctuation in the sensing layer in a well-designed ISFET as follows:

$$<\mathrm{i_n^2}> = \mathrm{g_m^2}\frac{\mathrm{e^2 N_0}}{\mathrm{fC^2 A}}\Delta\mathrm{f}$$

where N_0 is the areal density of active sites in the oxide layer contributing to charge fluctuation, *C* is the capacitance per unit area between the channel and electrolyte, *A* is the active sensing area of the device, f is the mean frequency within the bandwidth Δf of the electrical measurement circuit [6]. The SNR of the ISFET can be expressed as:

$$\mathrm{SNR} = \frac{\delta\varphi_0}{\frac{\mathrm{C^2 A}}{\mathrm{e^2 N_0}}\frac{\Delta\mathrm{f}}{\mathrm{f}} + \frac{<\mathrm{i_x^2}>}{\mathrm{g_m^2}}}$$

To maximize the SNR, *A* and g_m must be maximized [6]. The transconductance g_m is maximized in order to minimize the effect of $< i_x^2 >$ to achieve a noise performance that is intrinsic to the ISFET. Since, $g_m \propto \mu_{FET} C$, where μ_{FET} is the field effect mobility and *C* is the capacitance, the variables μ_{FET} and *C* should be maximized [6]. There are many ions whose concentration can be measured via ISFETs by simply modifying the sensing layer that has a strong selectivity to that specific ion [11]. These ions include H^+, Na^+, K^+, Ca^{2+}, Cl^-, F^-, NO^{3-}, and CO_3^{2-} [10]. In this thesis, we will only focus on three ions NH_4^+, Na^+, K^+ to highlight the enhanced resolution of graphene ISFETs for real-time and on-site measurements.

1.3 Graphene ISFETS

By incorporating graphene into ISFETs, the resolution is enhanced by a factor of ~10, and like all potentiometric sensors, measurements can be carried out on site and in real-time. More specifically, a graphene channel layer substitutes the silicon channel layer. This allows for the maximization of the channel area, the charge carrier mobility, and the capacitance between the ISFET channel and ion binding sites in order to minimize noise and improve the resolution. Finally, the fabrication process for large area-graphene ISFETs is simple due to a process that relies on chemical vapor deposition growth technique instead of traditional semiconductor growth methods [6], [12]. Figure 1.3 illustrates a picture of the graphene ISFET sensor that was used in this thesis.

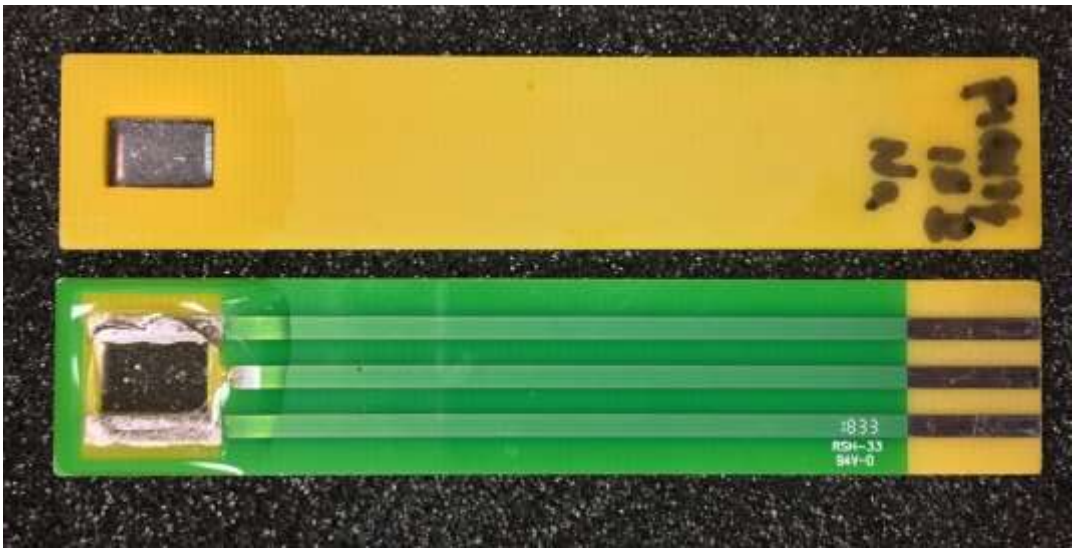

Fig. 1.3: A picture of a graphene ISFET

The sensor is made of a printed circuit board (PCB) with the graphene mounted on it. The sensor has a length of ~8 cm and width of ~1.5 cm. The ISFET itself is ~1x1 cm^2 with an active area of ~0.4 cm^2. Each sensor has a specific sensing layer that has a strong selectivity to the ion of interest [12]. The gate's top layer is made of an ion sensitive layer that enables ion binding events to modulate surface potential and thus transistor channel conduction [6].

The graphene layer is encapsulated with parylene C to protect the graphene FET channel from degradation during the deposition of sensing layers and to reduce hysteresis. Parylene C encapsulation also improves the long-term stability and reliability of the graphene ISFET. The detection layer is made of an ionophore that is sensitive to the ion in question. For example, to detect potassium ions in a solution, potassium ionophore III was used as the sensing layer [12]. The structure of the graphene ISFET sensor selective to K^+ is illustrated in Fig. 1.4 [12].

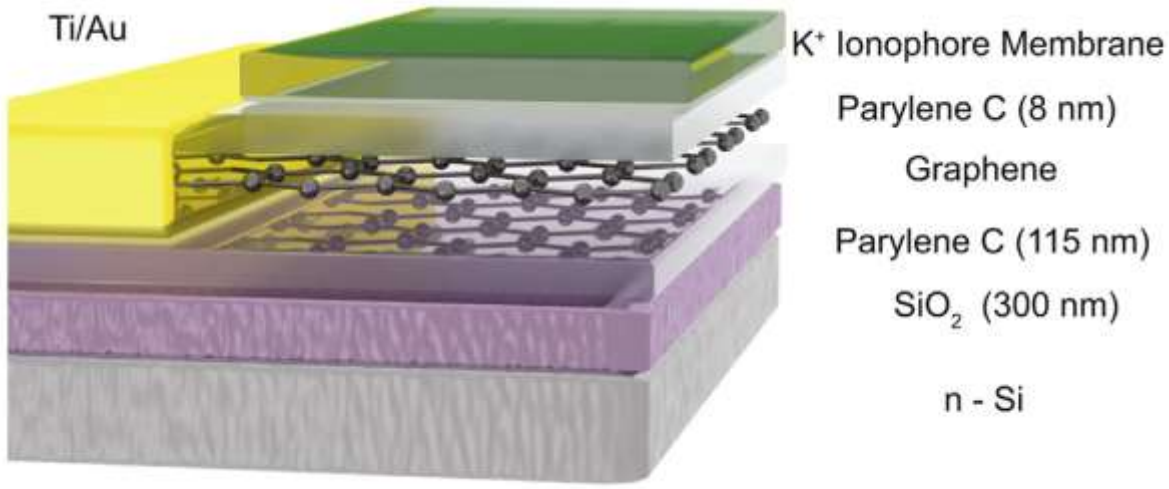

Fig. 1.4: A Cross-sectional schematic of graphene ISFET encapsulated with parylene and a layer of potassium ionophore membrane as a sensing layer on a Si-SiO_2 substrate. Note that this is only a schematic of the layers and shows only one electrical contact [12].

Two different kinds of large-area graphene-based ISFETs were demonstrated at McGill University with a metal oxide layer for protons (pH) and ionophore layers have been used for all other ions. We reproduced the same experiments from [6] and [12] for three ions NH_4^+, Na^+, K^+ using the same SPA, the Agilent Semiconductor Analyzer 1500B, to extract the sensitivity, resolution, detection limit, and RMS current fluctuation for each sensor. We reproduced the same experiments but by replacing the SPA with the portable device that we built and compared our results. Table 1.2 illustrates the results for protons and potassium ions that were established in these papers [6] and [12]. Fig. 1.5 illustrates a schematic of how the graphene ISFET is operated

Parameters	H^+	K^+
Resolution	0.1 mpH	2×10^{-3} log[K^+]
Sensitivity	55 mV/decade	37mV/decade
Detection limit	0.1 mpH	10^{-9} M
RMS current noise (in a 60Hz electrical bandwidth)	1 nA	5 nA

Table 1.2: The graphene ISFET parameters for hydrogen and potassium ion electrolyte [6], [12].

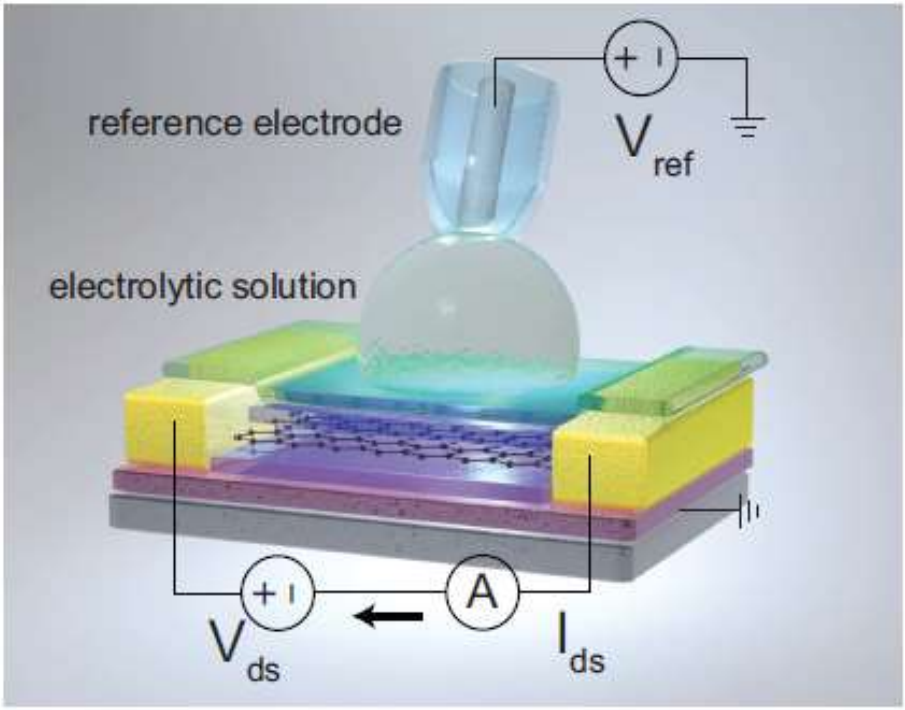

Fig. 1.5: An illustration of the bias setup for measuring the channel current for different molar concentrations. I_{ds} is the drain source current and V_{ds} is the drain source voltage [6].

In [6] and [12], the drain source current (I_{ds}) was measured, with the SPA, versus the electrolytic gate potential (V_{ref}), which is regulated through Ag/AgCl reference electrode at a constant drain-source bias voltage V_{ds}=100mV. The range of V_{ref} was controlled to prevent electrolysis of the analyte and to limit the current through the electrolytic gate to a maximum of 0.5% of the measured channel current I_{ds}. The ISFET's responses were measured by sweeping V_{ref} across

different molar concentrations. The results of this measurement are illustrated for K^+ ISFET sensor in Fig. 1.6. It can be clearly seen as the concentration of K^+ increases the transfer curve shifts uniformly and there is a decrease in the potential voltage at neutral point (V_{np}) required to reach charge neutrality. A V_{ref} is selected at a point where the largest number of curves intersect allowing for the largest range of molar concentration to be measured [6], [12]. In this thesis, we do not repeat this experiment, instead we rely on a more practical approach that will be discussed later to select V_{ref}.

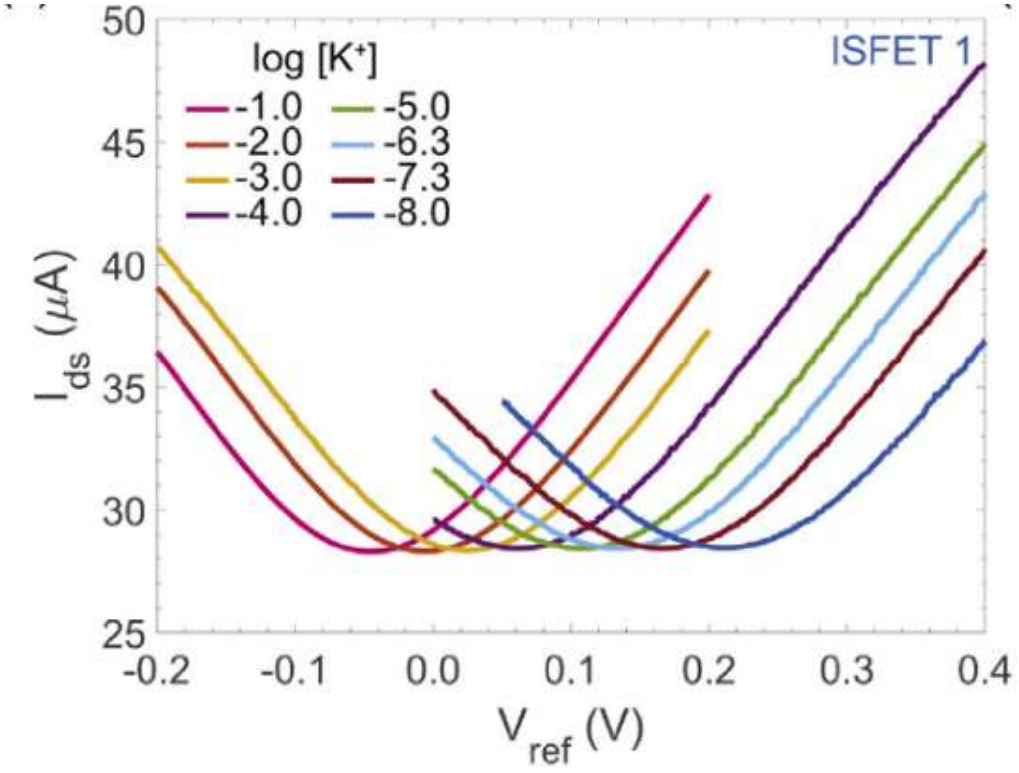

Fig. 1.6: The channel current, Ids of ISFET versus V_{ref} for different K+ molar concentrations [10].

The real-time response of graphene ISFETs to changes in molar concentration was also characterized. Fig. 1.7 illustrates this characterization for K^+ ISFET [12]. I_{ds} was measured versus time with a constant V_{ref} = 0V and V_{ds}=100mV as the K^+ concentration was varied [12]. The

concentration was increased decade wise at uniform time intervals from 10^{-10}M to 10^{-2} M which resulted in discrete current changes that range from 70 µA to 130 µA [6], [12]. Similarly, the interrogation circuit we developed for this project was primarily assessed by measuring the change in current as the molar concentration is increased decade wise at uniform time intervals from 10^{-7}M to 10^{-2} M. We carry this experiment out for three ISFET sensors that target three ions, Na^+, K^+, and NH_4^+.

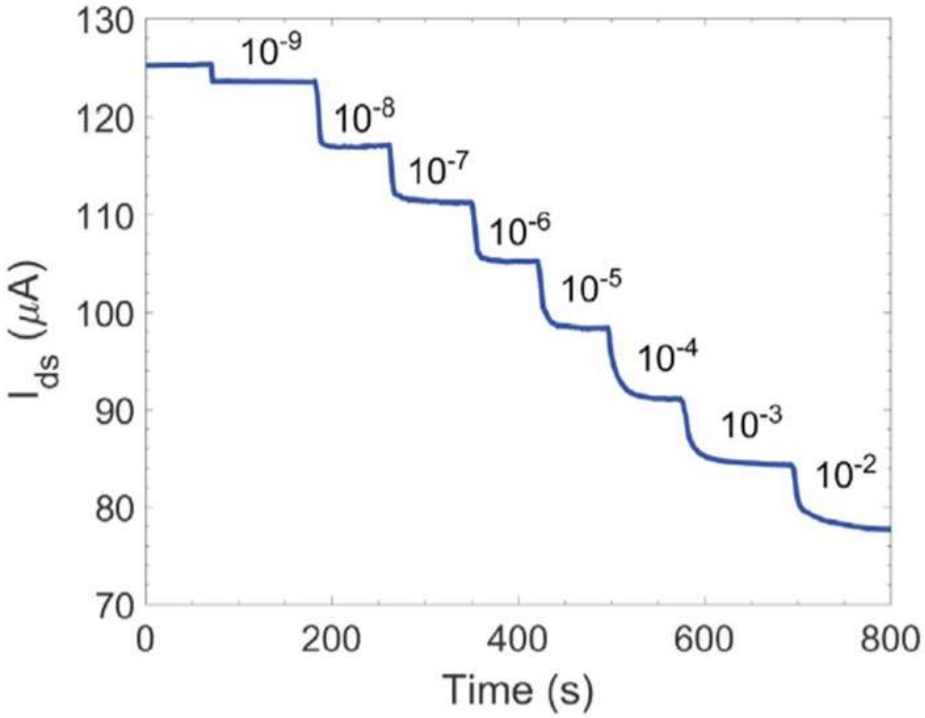

Fig. 1.7: A continuous real-time measurement of I_{ds} when increasing K^+ molar concentrations [12].

1.4 Rational for Selection of Analytes

Three graphene ISFETs that target K^+, Na^+, and NH_4^+ ions in a solution were selected because they are the most well-developed graphene ISFETs that were available for experimental work. The concentration of these ions is also important for environmental reasons.

NH_4^+ is one of the most important analytes for environmental sensing in fresh water. Ammonia exists in water in two primary forms; ionized NH_4^+ (or ammonium) and unionized NH_3, which are in equilibrium in water. Toxicity arises primarily from ammonia NH_3 and not ammonium NH_4^+. The relation equilibrium between the two is established by the chemical reaction:

$$NH_3 + H_2O \leftrightarrow NH_4^+ + OH^-$$

The ratio of ammonia to ammonium depends on temperature and pH. Fig. 1.8 illustrates the percentage of NH_3 in water at various pH levels and temperatures. As pH and temperature increases the relative concentration of NH_3 increases. The toxicity of ammonia is dependent on the organism and length of exposure. Fish are usually severly impacted due to the increase of ammonia concentration in large bodies of water such as lakes, rivers, and oceans. Ammonia contamination is typically attributed to several sources that include dumping of agriculture waste, industrial waste, and sewage water from sewage treatment plants [14].

pH	Temperature °C								
	16	18	20	22	24	26	28	30	32
7.0	0.29	0.34	0.39	0.46	0.52	0.60	0.69	0.80	0.91
7.2	0.46	0.54	0.62	0.82	0.83	0.96	1.10	1.26	1.44
7.4	0.73	0.85	0.98	1.14	1.31	1.50	1.73	1.98	2.26
7.6	1.16	1.34	1.55	1.79	2.06	2.36	2.71	3.10	3.53
7.8	1.82	2.11	2.44	2.81	3.22	3.70	4.23	4.82	5.48
8.0	2.86	3.30	3.81	4.38	5.02	5.74	6.54	7.43	8.42
8.2	4.45	5.14	5.90	6.76	7.72	8.80	9.98	11.29	12.72
8.4	6.88	7.90	9.04	10.31	11.71	13.26	14.95	16.78	18.77
8.6	10.48	11.97	13.61	15.41	17.37	19.50	21.78	24.22	26.80
8.8	15.66	17.73	19.98	22.41	25.00	27.74	30.62	33.62	36.72
9.0	22.73	25.46	28.36	31.40	34.56	37.83	41.16	44.53	47.91
9.2	31.80	35.12	38.55	42.04	45.57	49.09	52.58	55.99	59.31
9.4	42.49	46.18	49.85	53.48	57.02	60.45	63.73	66.85	69.79
9.6	53.94	57.62	61.17	64.56	67.77	70.78	73.58	76.17	78.55
9.8	64.99	68.31	71.40	74.28	76.92	79.33	81.53	83.51	85.30
10.0	74.63	77.35	79.83	82.07	84.08	85.88	87.49	88.92	90.19
10.2	82.34	84.41	86.25	87.88	89.33	90.60	91.73	92.71	93.58

Fig. 1.8: Percentage of NH_3 relative to total NH_3 and NH_4^+ at various pH and temperature in fresh water [15].

The concentration of K^+ and Na^+ are not as critical as NH_4^+ but monitoring their concentration in water is important. Na^+ is abundant in water due to its high solubility of many sodium salts. The dissolution of sodium chloride can be represented by the following chemical reaction:

$$NaCl(s) \rightarrow Na^+(aq) + Cl^-(aq).$$

The concentration of Na^+ varies from 30mg/L to 120mg/L depending on the location and type of body of water such as surface water or ground water and sea water or river water. As a result, very different organisms can survive in these different bodies of water. The Environmental Protection Agency (EPA) recommends that Na^+ in drinking-water not exceed 20 mg/L [16]. High concentration of Na^+ in water can be attributed to several reasons that include road salt, water treatment chemicals, domestic water softeners, sewage effluents, as well as the presence of water treatment chemicals [16].

Potassium is an essential element and is present in animals, humans, and plants. The primary source of potassium for humans is through food and water consumption. A survey from the World Health Organization indicates that the average concentrations of potassium in raw and treated drinking water in different areas vary between <1 and 8 mg/ in Canada, but concentrations of up to 51 mg/l in Saskatchewan were recorded [17]. Consuming a high dosage of potassium could result sever illness especially among infants due to their limited renal reserve and immature kidney function [17].

1.5 Original Contributions

In this thesis, we report the design and development of the portable device that we built which can operate graphene ISFETs on site and in real-time. The portable device is made up of three main parts; the interrogation circuit, the case of the interrogation circuit, and the case of the graphene ISFET. We demonstrate the interrogation circuit that we built which is used to bias a graphene ISFET and measure I_{ds}. The I_{ds} measurement correlates to a molar concentration of the target ion. The interrogation circuit is operated via a wireless connection using secure shell (SSH) connection and is powered by a 24 Ah battery bank which allows us to power the interrogation circuit for over 40 hours before needing to recharge. We also present the 3D printed case that holds the graphene ISFET sensor in place with the reference electrode and provides the proper electrical wiring to the graphene ISFET. We also present the case that we assembled that holds the interrogation circuit.

We evaluated the performance of the portable device using three graphene ISFET sensors that target K^+, Na^+, and NH_4^+ ions in a solution. Table 1.3 illustrates the performance of the portable device in terms of the detection limit, sensitivity, I_{ds} RMS fluctuation (ΔI_{ds}), resolution, and I_{ds} range ($I_{ds\text{-}range}$) for each graphene ISFET.

ISFET sensor ion detection	Detection limit (log(M))	Sensitivity, S (µA/decade)	I_{ds} RMS fluctuation, ΔI_{ds} (µA)	Resolution, R (Log(M))	I_{ds} range, $I_{ds\text{-}range}$ (µA)*
K^+	-6.5	-8.04	0.11	0.014	87.94-52.41
Na^+	-6.5	-12.89	0.17	0.013	129.14-71.34
NH_4^+	-5.5	-21.36	0.13	0.0061	199.95- 119.16

Table 1.3: The detection limit, sensitivity, I_{ds} RMS-fluctuation, resolution, and mean I_{ds} range for K^+, Na^+, and NH_4^+ sensitive ISFET sensors

* $I_{ds\text{-}range}$ is for a log molar concentration range of -6.5 to -2

A calibration function was generated for each graphene ISFET that correlates I_{ds} and the molar concentration. The calibration functions were used in real-time to report the I_{ds} measurements in terms of the molar concentration on the IoT platform https://thingspeak.com/. We present the real-time and on-site measurements of a demo that we conducted for Ericsson at their office in Ville Saint Laurent, Quebec, Canada on the IoT platform.

1.6 Thesis organization

The thesis is organized into the following chapters, described below.

Chapter 2: Molar Concentration Measurements via SPA

In this chapter, we summarize the setup and results for calibrating and measuring the molar concentration of three ISFET sensors that target K^+, Na^+, and NH_4^+ ions in a solution using a SPA. We generated a series of I_{ds} versus time curves and I_{ds} versus molar concentration curves to extract the detection limit, sensitivity, I_{ds} RMS fluctuation, resolution, and I_{ds} range for each graphene ISFET.

Chapter 3: Portable Device Design

In this chapter, we present the portable device that we built as an on-site alternative to the SPA presented in Chapter 2. We present each part of the portable device which is a compact and integrated solution that includes: 1. interrogation circuit to measure and supply voltages/currents to an ISFET sensor 2. a case that holds the interrogation circuit 3. a case that holds the ISFET sensor and reference electrode. We discuss each one of these parts in rigorous details in this chapter and we present the IoT platform that we used to post our measurements in real-time.

Chapter 4: Molar Concentration Measurements via Agilent B1500A

In this chapter, we summarize the setup and results for calibrating and measuring the molar concentration of three ISFET sensors that target K^+, Na^+, and NH_4^+ ions in a solution using the portable device. We generated a series of I_{ds} versus time curves and I_{ds} versus molar concentration curves to extract the calibration function and evaluation metrics which include; the detection limit, sensitivity, I_{ds} RMS fluctuation, resolution, and I_{ds} range for each graphene ISFET. We then compared the evaluation metrics results of the SPA to portable device.

2. Molar Concentration Measurements via Agilent B1500A

2.1 Introduction

In this chapter, we summarize the setup and results for calibrating and measuring the molar concentration response of three graphene ISFET that target K^+, Na^+, and NH_4^+ ions in a solution to compare the ISFET sensors' behavior to the interrogation circuit that we built. We increased the ion concentration of the analyte gradually by adding a higher concentration solution to it (this process is referred to as "spiking" the analyte). As the solution is spiked, we measured the I_{ds} of the graphene ISFET versus time. We then generated a series of I_{ds} versus time curves and I_{ds} versus molar concentration curves to extract the detection limit, sensitivity, resolution, and I_{ds} range for each sensor. It is important to note here, that the detection limit, sensitivity, resolution, and I_{ds} range are properties of the sensor. However, the current range is a variable that is important for the design of the biasing circuit.

The measurements were conducted via a well-known instrument in the field of semiconductors, known as an SPA. More specifically, we used the Agilent B1500A SPA. The Agilent B1500A is an integrated solution for semiconductor device DC/AC parametric measurement and analysis applications [14]. We selected this device for two reasons. First, the Agilent B1500A can provide an AC and DC voltage/current output as well as an AC and DC voltage/current measurement [14]. This allowed us to measure the change in I_{ds} as the ion concentration of the test solution is increased and to supply the biasing voltage to the source, drain, and electrode terminals of the

ISFET sensor. The second reason is that the Agilent B1500A is a very low noise measurement device [14]. Table 2.1 illustrates the current measurement resolution of the SPA [14]. As stated in Chapter 1 the I_{ds} range is expected to lie between 50µA and 200 µA with a current resolution of 1nA [6] [10]. From Table 2.1 we can see that we are within the required resolution limit for the sensors [14]. Thus, the inherent noise that is introduced in our measurements is predominantly from the sensor. Fig. 2.1 is a picture of the Agilent B1500A that we used to run our experiments. We describe the experimental setup and results in the next two sections, respectively.

Range	Resolution
±1 pA	0.1 fA
±10 pA	1 fA
±100 pA	2 fA
±1 nA	10 fA
±10 nA	10 fA
±100 nA	100 fA
±1 µA	100 fA
±10 µA	100 fA
±100 µA	100 pA
±1 mA	1 nA

Table 2.1: The Agilent B1500A Measurement Resolution for Various Current Ranges [18]**.**

Fig. 2.1: The Agilent Technologies B1500A SPA that was used for measuring I_{ds} versus time as the concentration of the analyte is increased.

2.2 Experimental Setup

In this section, we present the methodology and discuss the steps for calibrating and measuring the molar concentration of three ISFET sensors to target K^+, $Na^{+,}$ and NH_4^+ ions in a solution. Fig 2.2 is an illustration of our experimental setup. The graphene ISFET and reference electrode are submerged in the analyte held in a beaker, ensuring that the sensing layer is fully submerged. We connected the source measurement units (SMUs) of the SPA to the source and drain of the ISFET sensor and reference electrode using the sensor holder. The SMUs measures and supplies voltages and/or currents. We used them explicitly to supply 0.1 V to the source, 0 V to the drain, 0.1 V to the reference electrode, and we measured I_{ds}. V_{ref} is set to 0.1 V to ensure the ISFET remains in the linear region of its operation to capture the largest change of molar concentration

that is reflected by I_{ds}. V_{ds} is set to 0.1V to minimize the required current to operate the sensor. Fig. 2.3a-b are pictures of our setup that shows how the sensor holder encloses the graphene ISFET and reference electrode with the cables that are connected to the SPA.

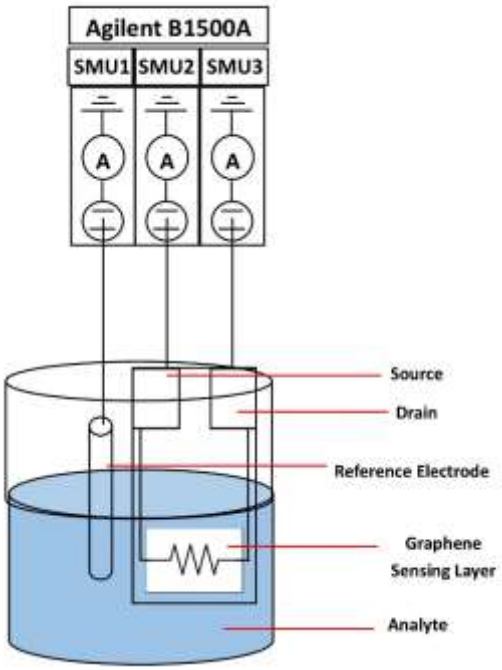

Fig. 2.2: An illustration of the connections of the SPA (Agilent B1500A) to the graphene ISFET and reference electrode in the analyte.

(a) **(b)**

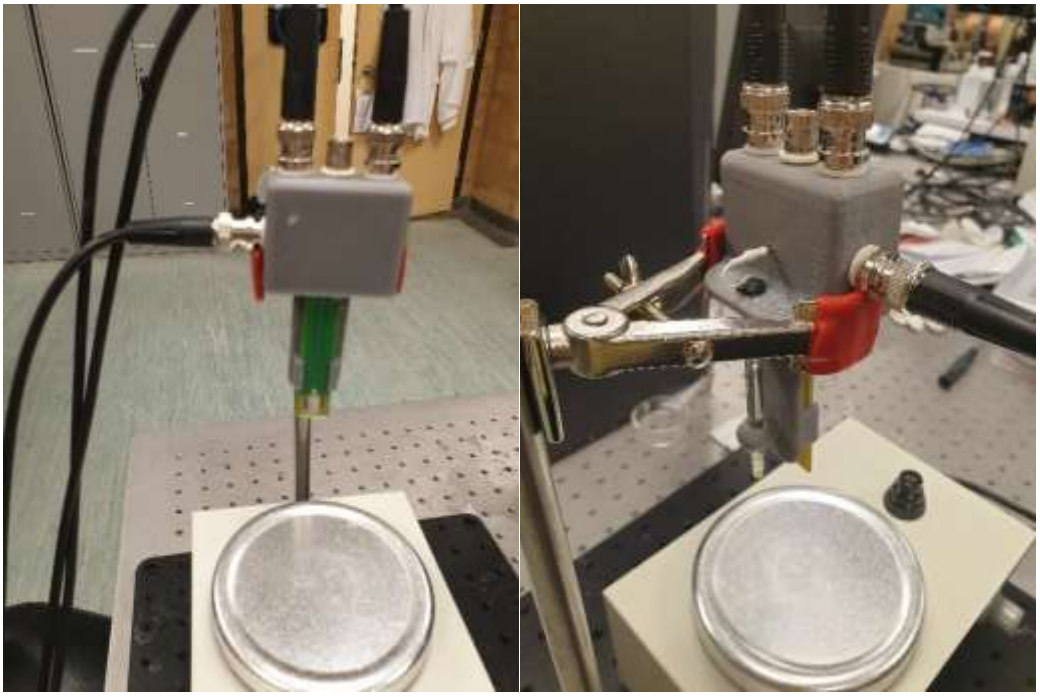

Fig. 2.3: The sensor holder with the ISFET sensor and reference electrode (a) front view (b) side view.

We prepared ~200 mL stock solutions of 10^{-5}, 10^{-4}, 10^{-3}, 10^{-2}, 10^{-1}, and 1 M of NaCl, KCl, and NH_4Cl. This was done through the dilution process. We began by making the highest molar concentration solution, 1 M, by diluting the solute in DI water. To calculate the required mass of the solute we use the following equations (using NaCl as an example):

$$\text{Molar concentration (mol L}^{-1}) = \frac{\text{Mass of solute (g)}}{\text{Molar mass (g mol}^{-1}) * \text{Volume of solution (L)}}$$

$$1 \text{ mol L}^{-1} = \frac{\text{Mass of solute (g)}}{\text{Molar mass (g mol}^{-1}) * \text{Volume of solution (L)}}$$

$$\text{Mass of solute} = 1 \text{ mol L}^{-1} * (58.44 \text{ g mol}^{-1} * 0.2\text{L})$$

$$\text{Mass of solute} = 11.688\ \text{g}$$

To prepare the remaining molar concentration, we use the molar concentration stock solution that is one order of magnitude larger than our target molar concentration and diluted it in DI water. For example, to prepare 10^{-1} M stock solution we diluted 1 M stock solution in DI water. To determine the exact quantity of the added molar concentration stock solution and DI water, we used the following formulae:

$$C_{\text{initial}} * V_{\text{initial}} = C_{\text{final}} * V_{\text{final}}$$

$$1\text{M} * V_{\text{initial}} = 0.1\text{M} * 0.200\ \text{L}$$

$$V_{\text{initial}} = \frac{0.1\text{M} * 0.200\ \text{L}}{1\ \text{M}} = 0.02\ \text{L} = 20\ \text{mL}$$

$$V_{\text{DI water}} = V_{\text{final}} - V_{\text{initial}} = 200\ \text{mL} - 20\text{mL} = 180\ \text{mL}.$$

We begin our measurement of I_{ds} with DI water and increase the molar concentration of analyte in a logarithmic fashion with half decade steps (increase in concentration by a factor of $10^{0.5}$ for each step) every ~3 minutes until the analyte reaches a molar concentration of 10^{-1} M. Increasing the molar concentration of the analyte is done by adding the proper concentration and volume of stock solution. We have created a MATLAB script (presented in section A. 1) to calculate the volume of stock solution required for a given initial analyte molar concentration and volume, the desired molar concentration, and the stock solution molar concentration.

We used a pipette to add the stock solution to the analyte to ensure that we are adding the precise amount determined. In general, we used a stock solution that is two orders of magnitude higher than the target molar concentration of the analyte to minimize the volume of stock

solution we add to prevent the analyte in the beaker from overflowing. Table 2.2 illustrates the initial volume and molar concentration of the analyte, the volume and molar concentration of the added solution, and the final molar concentration of the analyte after adding the stock solution in our experiment. In the next section, we present and discuss the results from this experiment.

Sample Number	Initial Volume of Analyte (µL)	Initial Molar Concentration of Analyte (log(M))	Added Volume of stock solution (µL)	Added Stock solution Concentration (log(M))	Final Molar Concentration of Analyte (log(M))
1	45000	DI water	455	-5	-7
2	45455	-7	100	-4	-6.5
3	45555	-6.5	315	-4	-6.0
4	45870	-6.0	1025	-4	-5.5
5	46895	-5.5	325	-3	-5.0
6	47220	-5.0	1055	-3	-4.5
7	48275	-4.5	335	-2	-4.0
8	48610	-4.0	1085	-2	-3.5
9	49695	-3.5	345	-1	-3.0
10	50040	-3.0	1115	-1	-2.5
11	51155	-2.5	355	0	-2.0
12	51510	-2.0	1150	0	-1.5
13	52660	-1.5	4000	0	-1.0

Table 2.2: The initial volume and molar concentration of the analyte, the volume and molar concentration of the added stock solution, and the final molar concentration of the analyte after adding the stock solution for the SPA.

2.3 Results and Discussion

In this section, we present and discuss our results for measuring I_{ds} as the molar concentration of the analyte is increased. Fig. 2.4a-c illustrate our measurements of I_{ds} versus time as we increased the molar concentration of the analytes KCl, NaCl, and NH_4Cl, respectively. We began our measurment with a concetration of 10^{-7} M and increased it to 10^{-1} M in a logarithmic fashion with

half decade steps (increase in concentration by a factor $10^{0.5}$ for each step). Each transient spike in I_{ds}, in Fig. 2.4a-c, indicates the addition of the stock solution that increases the molar concentration of the analyte. Over time, the added stock solution establishes a new equilibrium analyte concentration and a new equilibrium I_{ds}. Fig. 2.4a-c all show a decrease in I_{ds} over time as the molar concentration of the anaytle increases. However, the range varies slightly for each analyte. From Fig 2.4a we can see I_{ds} ranging from ~140µA to ~70µA for KCl, from Fig 2.4b we can see I_{ds} ranging from ~140µA to ~110µA for NaCl, and Fig 2.4c we can see I_{ds} ranging from ~140µA to ~90µA for NH_4Cl.

(a)

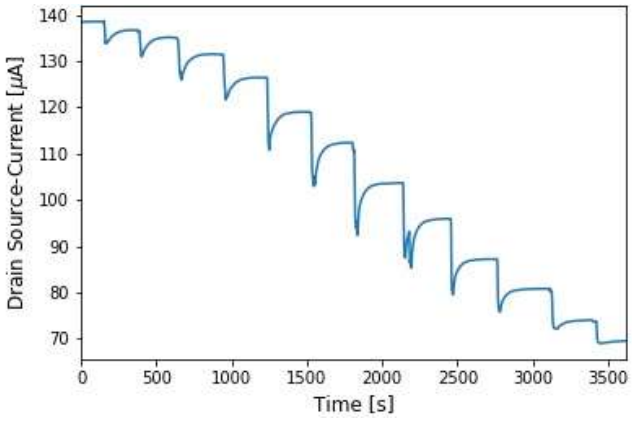

(b)

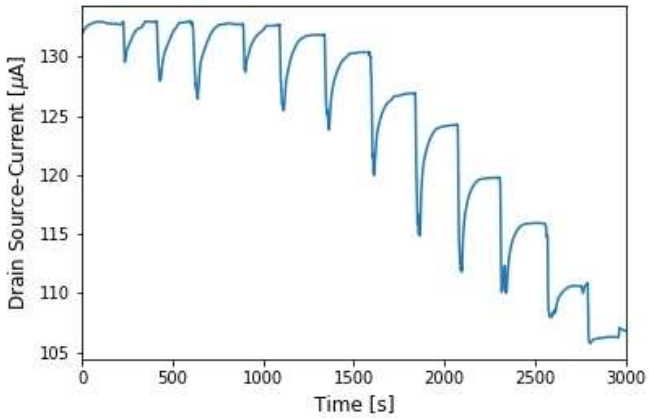

(c)

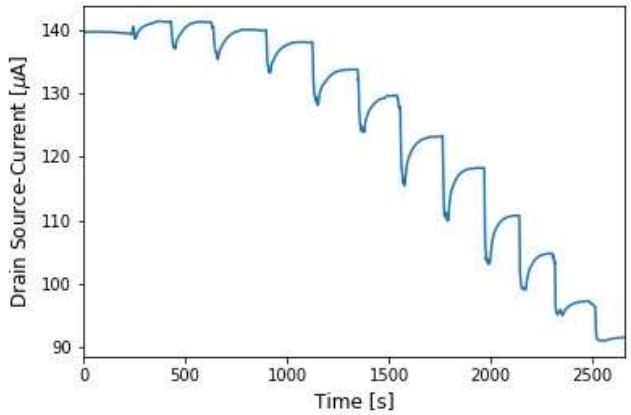

Fig. 2.4: I_{ds} versus time of the target ion (a) K^+ (b) Na^+ (c) NH_4^+ sensitive ISFET as the molar concentration of the analyte is increased. Each spike on the graph indicates the addition of stock solution to increase the concentration of the analyte by half-decades, from 10^{-7} M to 10^{-1} M.

From Fig. 2.4a-c we generated Fig. 2.5a-c that illustrates the mean I_{ds} versus molar concentration of each analyte in a logarithmic scale for KCl, NaCl, and NH_4Cl, respectively. It should be noted here when calculating the mean we only used the steady state values of I_{ds} at each molar concetration, which coresponds to the last ~120 seconds of the measured I_{ds} at a fixed molar concentration. The transient spikes were disregarded because they correspond to the mixing process of the analyte with the stock solution. From the data presented in Fig. 2.5a-c we extracted the sensitivity, detection limit, and resolution of each graphene ISFET and we present them in Table 2.3. We also present the I_{ds} RMS fluctuation (ΔI_{ds}) and the I_{ds} range ($I_{ds\text{-}range}$) for each ISFET sensor using the data from Fig. 2.4a-c. Each parameter is defined in Table 2.3. We will use Table 2.4 in chapter 4 to compare the performance of the portable device and SPA for the graphene ISFETs. In the next chapter, we discuss the design and development of the portable device.

(a)

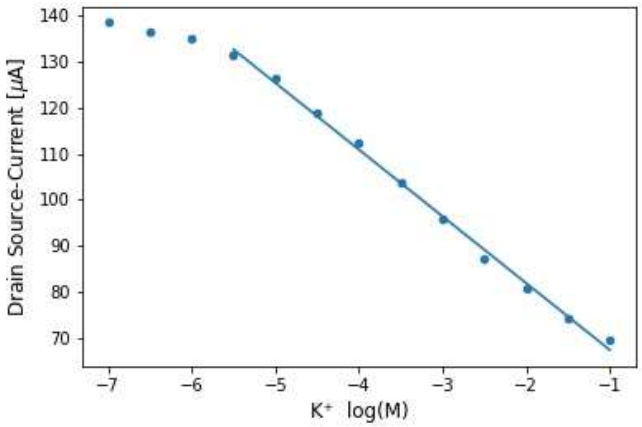

(b)

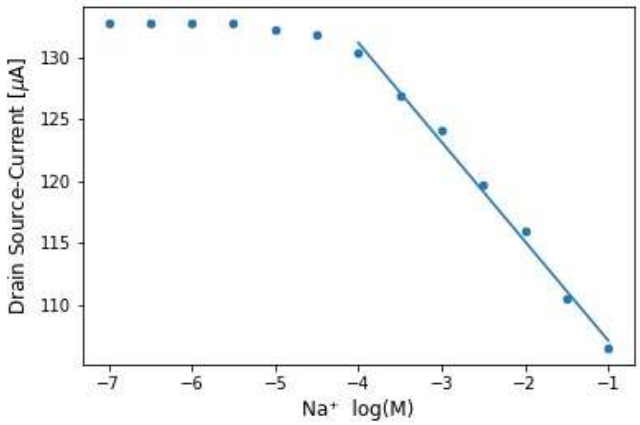

(c)

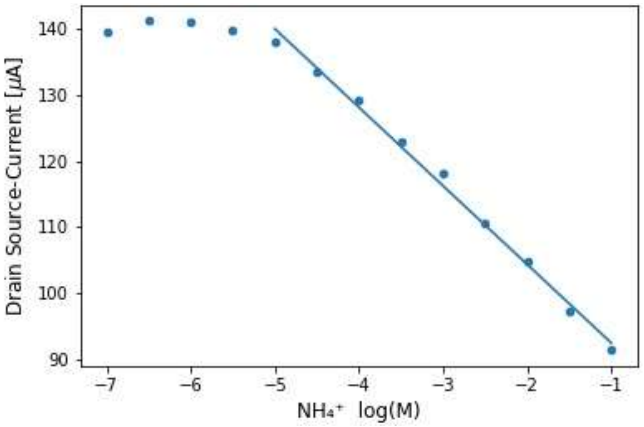

Fig. 2.5: I_{ds} of the (a) K^+ (b) Na^+(c) NH_4^+ sensitive ISFET versus log(molar concentration) of the analyte as we increased the concentration of the analyte by half-decades, from 10^{-7} M to 10^{-1} M. (a) **S:** -14.54 µA/dec **ΔI_{ds}**: 0.04 µA (b) **S:** -8.01 µA/dec **ΔI_{ds}**:0.14 µA/dec (c) **S:** -11.92 µA/dec **ΔI_{ds}**: 0.10 µA

$S = \frac{d\overline{I_{ds}}}{d(log(a))}$	where a is the molar concentration
$D = log(c) \mid S(c) = \frac{1}{2}\max(S)$	
$\Delta I_{ds} = \frac{1}{P}\sum_{p=0}^{P}\left(\sqrt{\frac{1}{N}\sum_{n=1}^{N}\{(I_{ds})_n - \overline{I_{ds}}\}^2}\right)_p$	where P is the number of fixed molar concentration, N is the number of I_{ds} measurements, and $\overline{I_{ds}}$ is mean of the I_{ds} measurements
$R = \frac{\Delta I_{ds}}{S}$	
$I_{ds-range} = \max(\overline{I_{ds}}) \; and \; \min(\overline{I_{ds}})$	

Table 2.3: The definitions of the evaluation metrics of graphene ISFET sensor response.

ISFET sensor ion detection	Detection limit (log(M))	Sensitivity, S (µA/decade)	I_{ds} RMS fluctuation, ΔI_{ds} (µA)	Resolution, R (Log(M))	I_{ds} range, $I_{ds\text{-}range}$ (µA)*
K^+	-5.5	-14.54	0.04	0.002	138.52- 69.38
Na^+	-4	-8.01	0.14	0.017	132.81 - 106.5
NH_4^+	-5	-11.92	0.10	0.0084	139.58 – 91.41

Table 2.4: The detection limit, sensitivity, I_{ds} RMS-fluctuation, resolution, and mean I_{ds} range for K^+, Na^+, and NH_4^+ sensitive ISFET sensors.

* $I_{ds\text{-}range}$ is for a log (molar concentration) range of -7 to -1

3. Portable Device Design

3.1 Introduction

In this chapter, we present the portable device that we built as an on-site alternative to the SPA presented in Chapter 2. The portable device is a compact and integrated solution that includes an interrogation circuit to measure and supply voltages/currents to an ISFET sensor, a case that holds the interrogation circuit, and a case that holds the ISFET sensor and reference electrode. Fig. 3.1 is a picture of the portable device that we built (with an ISFET sensor connected to it) and used for conducting our experiments. Fig. 3.2 is an illustration of the different parts of the portable device. In Fig. 3.2, we display the two main components of the interrogation circuit, the control board and the expansion board. The control board is a Raspberry Pi 3 – Model B board which is a single board computer (SBC). The expansion board is a series of ICs that include a transimpedance amplifier circuit, two digital to analog converters (DACs), an analog to digital converter (ADC), and three connectors to connect a graphene ISFET. The expansion board realizes functionality that the SBC cannot achieve that are required for our experiments. The interrogation circuit is operated through the SBC, either by directly programing it or via secure shell (SSH) connection from any smart device such as a smart phone or laptop. In Fig. 3.2, we also display the ISFET sensor holder that is connected to the interrogation circuit via a ribbon cable and a power supply cable that is connected to an external power source. In the next sections, we present and discuss the valuable insights of the control board, the expansion board, the circuit interrogation case and the ISFET sensor case.

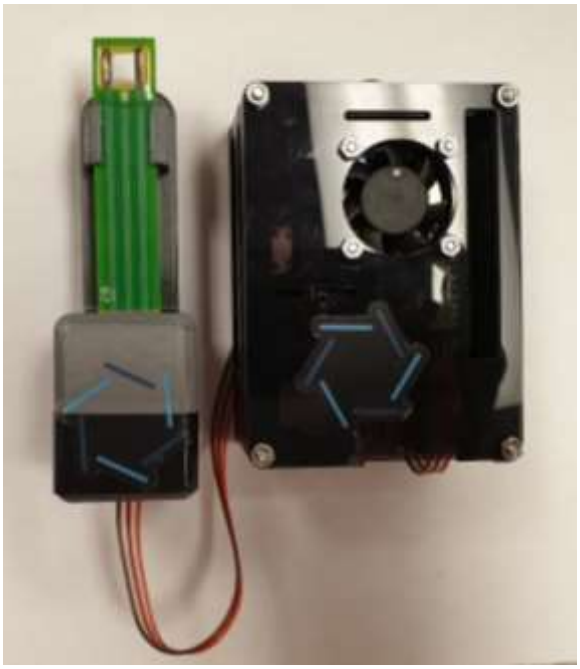

Fig. 3.1: The portable device that is made up of the interrogation circuit and its case and the ISFET sensor case with an ISFET sensor connected to it.

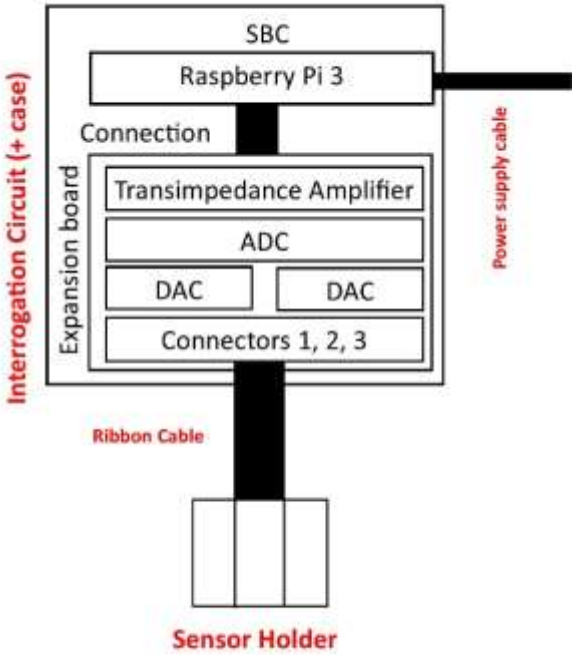

Fig. 3.2: An Illustration of the portable device that shows the interrogation circuit (SBC + expansion board) and the ISFET sensor holder.

3.2 Control board – Single Board Computer

In this section, we discuss the reasons for selecting the Raspberry Pi 3 – Model B as the controller board for the interrogation circuit. The Raspberry Pi 3 – Model B is an SBC that can be programmed to read/write digital signals to/from its general purpose input/output (GPIO) pins. Fig. 3.3 is a picture of the Raspberry Pi 3 – Model B with the key components labeled and a GPIO pinout diagram.

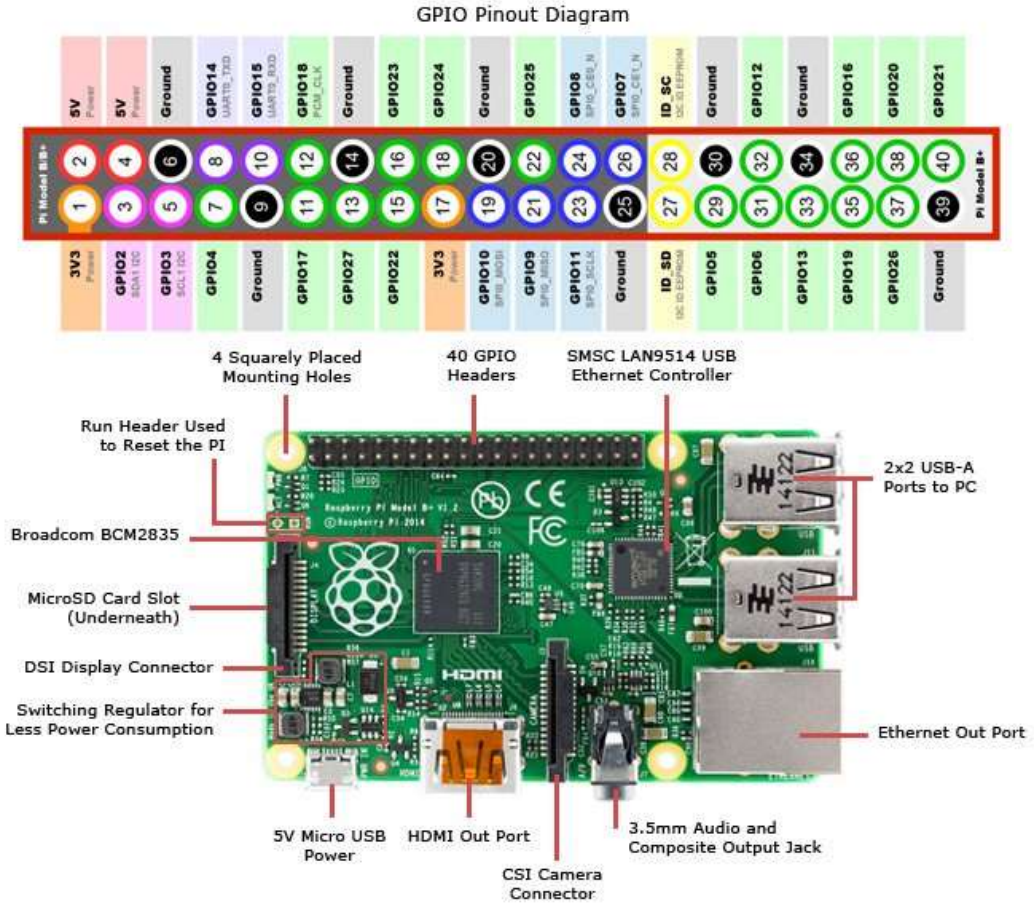

Fi**g. 3.3:** A picture of the Raspberry Pi 3 – Model B with the main components labeled and a GPIO pinout diagram [19].

This SBC has a Debian-based (i.e. Linux Kernel) operating system (OS) which made it easy for us to program and operate the interrogation circuit. A controller board with an OS installed on it, enabled us to program the interrogation circuit directly. Specifically, we did not need a connection to another computer to upload the code onto the controller board. Additionally, having an OS made it possible for us to carry out all the programing of the interrogation circuit in Python, which is a high-level programing language, that makes the programing process easier and more user friendly. An OS is required because a Python interpreter and complier must be installed to run Python scripts. Additionally, there were several open source libraries that were available to us that made the programing process easier.

To communicate between the SBC and the ICs on the expansion board we used Inter-integrated circuit (I2C) communication protocol. I2C communication protocol is a serial communication protocol that allows the SBC to send and receive data, to and from the ICs on the expansion board along the SDA (serial data) line while synchronizing the clock speed along the SCL (serial clock) line. The data being sent to the ICs is their configuration and settings, and the data received by the SBC is the measurements conducted by the ICs [20], [21], [22], [23]. The GPIO2 and GPIO3, pin 3 and 5 in Fig 3.3, are the two GPIO pins on the SBC dedicated for SDA and SCL lines that we used

All the ICs on the expansion board require a 3.3 V voltage supply and GND connection which we supply through the 3.3 V voltage supply pin (pin 1) and GND (pin 6) that are illustrated in Fig 3.3. The SBC is powered via a 5 V micro USB port, that then powers the expansion board via the 3.3 V pin and GND pin. We used a 24 Ah waterproof portable battery bank that can power the

portable device for more than 40 hours which enabled us to conduct on-site measurements. Fig 3.4 is a picture of the portable device with the power bank connected to it.

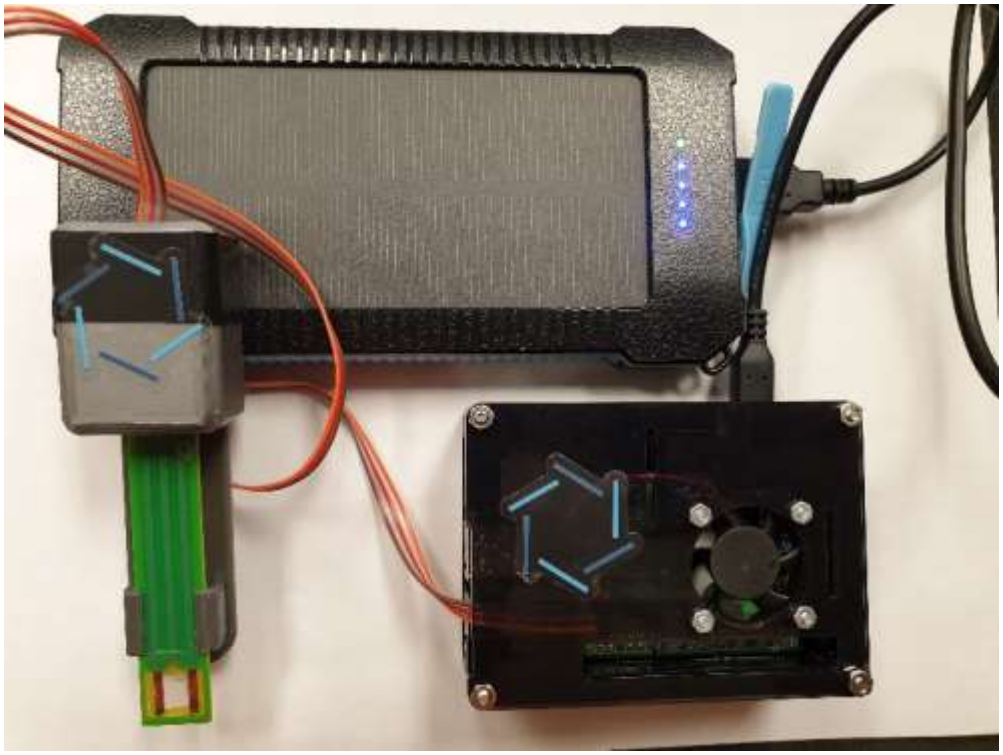

Fig. 3.4: The portable device powered by a 24 Ah waterproof portable battery bank.

The SBC has an 802.11n Wireless LAN adapter that allowed us to operate the interrogation circuit over the same Wi-Fi network using a smart phone/laptop [24], [25]. The communication between the SBC and the smart phone or laptop is carried out using SSH, which is a cryptographic network protocol for operating network services securely over an unsecured network [26], [27]. Upon connection, we ran Linux commands and programmed python scripts in the terminal.

Finally, the portable device was incorporated into an internet of things (IoT) platform. IoT is a network or system that incorporates devices capable of interacting with each other. These devices can be as small as a photonic sensor and as larger as a drone or vehicle. Usually, the devices on an IoT platform are placed in two categories: sensors and/ or actuators. Sensors are devices that convert physical parameters into an electric signal such as converting the temperature measured by a thermometer into a digital signal and actuators are devices that convert electrical signals into a physical output such as triggering an electric motor. However, the concept of IoT is continuously evolving where we see new types of devices such as servers, routers, and cloud platforms. These networks can hold as little as two devices and as many as millions of devices [28], [29], [30] .

For the scope of this thesis, we used an online IoT platform called ThingSpeak (https://thingspeak.com/) which is an IoT platform service that allowed us to collect, visualize, and analyze live data streams of the measured molar concentration from different graphene ISFETs. On this IoT platform, we created a unique channel that hosts an interactive dashboard which stores and visualizes the measured molar concentrations from our experiments in real-time. The interactive dashboard displays a graph of the log molar concentration versus time, and a numerical display of the most recent log molar concentration measurement of each graphene ISFET. Fig. 3.5 is screenshot of the interactive dashboard. The data displayed are measurements conducted in real-time and on-site using the portable device at the Ericsson office in Ville Saint Laurent, Quebec, Canada. We discuss the results of the experiments in Chapter 4.

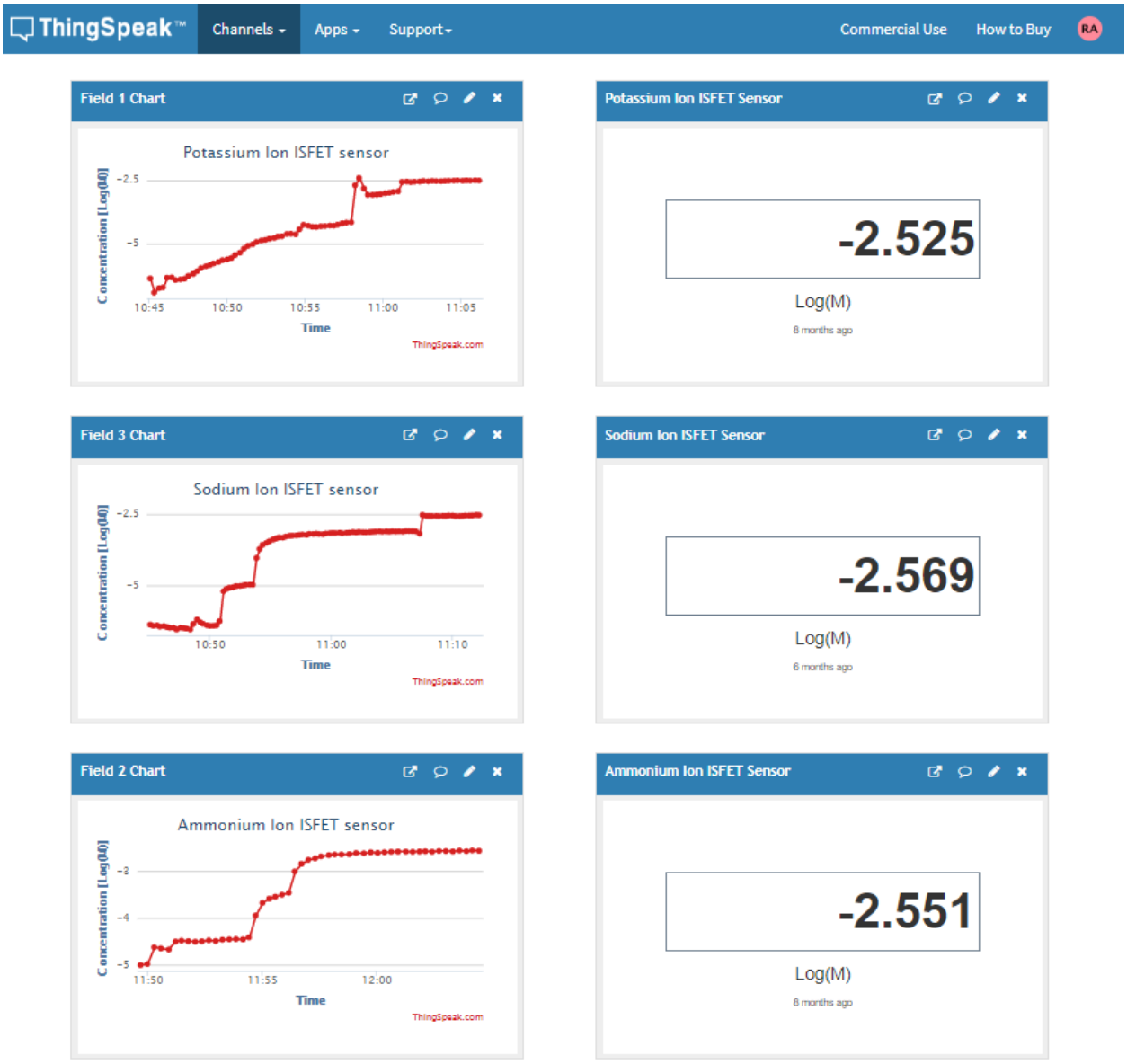

Fig. 3.5: A screenshot of the interactive dashboard on the IoT platform https://thingspeak.com/. On the right side, the log molar concentration versus time plot is displayed for each graphene ISFET. On the right side, a numerical display of the most recent log molar concentration measurement is displayed for each graphene ISFET. The data displayed are measurements conducted in real-time and on-site using the portable device at the Ericsson office in Ville Saint Laurent, Quebec, Canada.

We now turn our attention to the physical aspects of the device including its case. The SBC is a small and compact device with the following dimensions; 85.6 x 56.5 x 11 mm and weight ~45g

[31]. Thus, the SBC is small and light enough to be an ideal solution for on-site measurements. The SBC board also has four screw mounting holes which we used to attach the case we created for the interrogation circuit. The case was made by combing two Raspberry Pi 3 Model B Smraza Compatible cases to create vertical space for the expansion board [32]. The vertical space is needed because the expansion board is mounted on the top of the GPIO pin by sliding the female headers of the expansion board onto of all 40 of the GPIO pins as illustrated Fig. 3.6. Fig. 3.7a is a picture of an SBC board enclosed in its case. Fig. 3.6b is a picture of the interrogation circuit enclosed in the case we created by combining Raspberry Pi 3 Model B Smraza Compatible cases board [32].

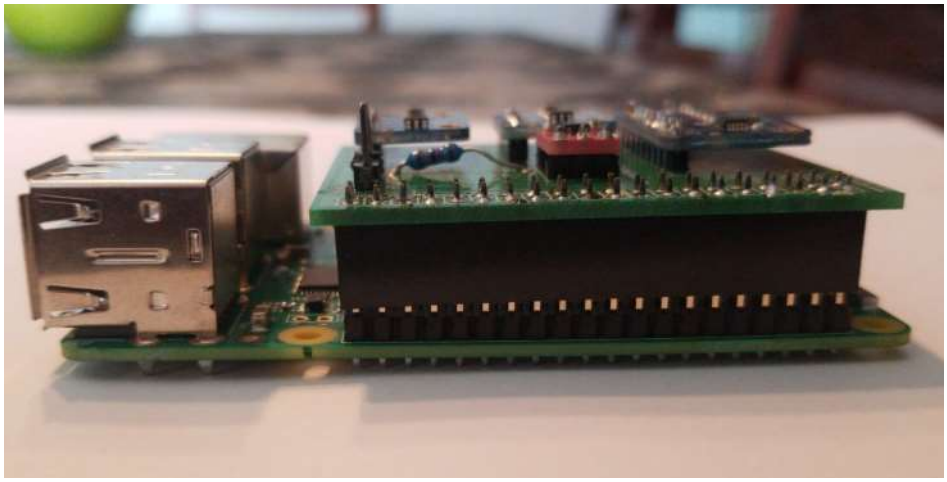

Fig. 3.6: A picture of the expansion board that is pinned on the GPIO pins of the Raspberry Pi-Model B.

(a)

(b)

Fig. 3.7: (a) A picture of an SBC board enclosed in its case [32]. (b) A picture of the interrogation circuit enclosed in the case we created by combining the Raspberry Pi 3 Model B Smraza Compatible cases [32].

The SBC replicates most of the required functionalities of the SPA. However, the SBC cannot produce analog signals, which are required to bias the ISFET sensor. The SBC also cannot measure the current I_{ds} which is essential to the sensor's operation. In the next section, we discuss the

expansion board that we created to fulfill the remaining functionalities required to operate the ISFET sensor.

3.3 Expansion Board:

In this section, we discuss the architecture of the expansion board and how it builds on the functionality of the SBC to operate the ISFET sensor. More specifically, we present the layout of the board and discuss how the board enabled us to measure I_{ds} and supply the bias voltage to the ISFET sensor. Fig 3.8 is a picture of the expansion board and Fig. 3.9 is the printed circuit board (PCB) layout of the expansion board that we designed and that was manufactured at a commercial facility. All the ICs were soldered on the top of the PCB, except for the 20 x 2 female pin header, which was soldered at the bottom of the PCB as illustrated in Fig. 3.8. The female headers are connected directly to the GPIO pins of the SBC as illustrated in Fig. 3.6. They are used to hold the expansion board to the SBC without contacting other parts of SBC board. Additionally, we used four pins from the SBC board to operate the expansion board. We used the 3.3 V and GND pins to power the ICs and the SCL and SDA pins to communicate with the ICs via I2C communication protocol. Fig. 3.9 is the schematic of the expansion board where we can see the connections between the pins and the ICs.

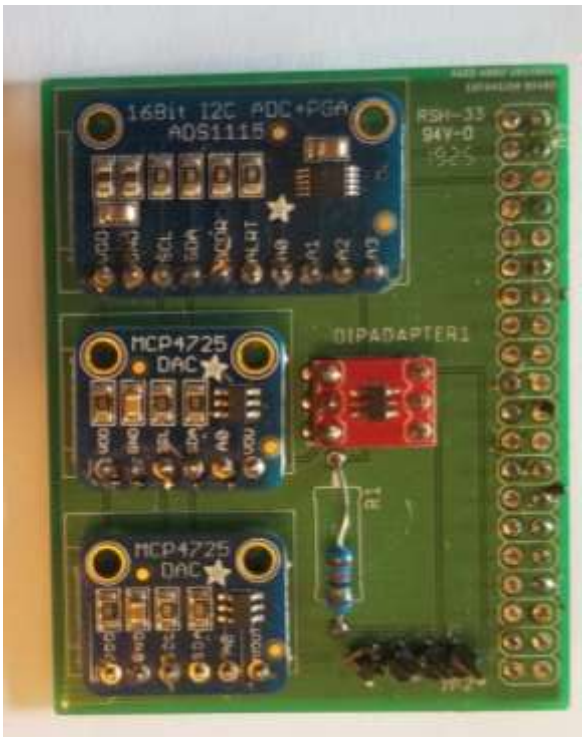

Fig. 3.8: The expansion board of the interrogation circuit with all the parts soldered on it.

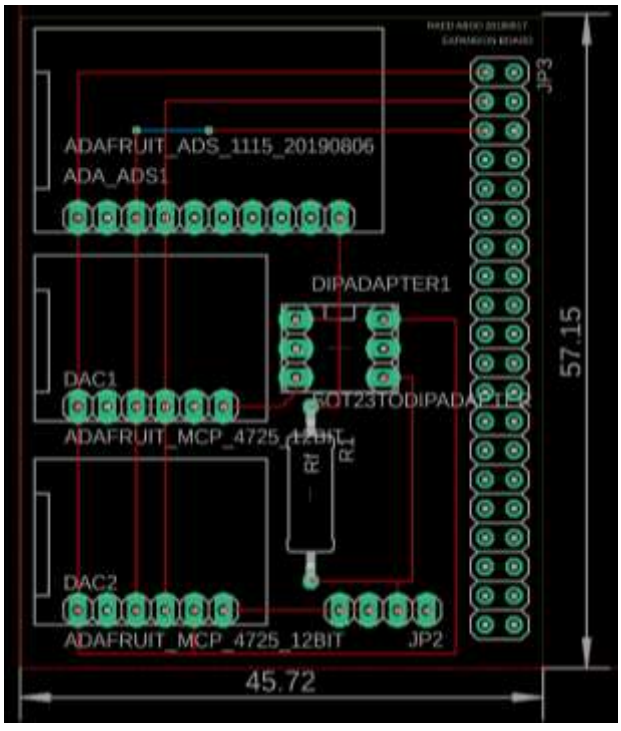

Fig. 3.9: The PCB board layout of the expansion board with the measurements in millimeters.

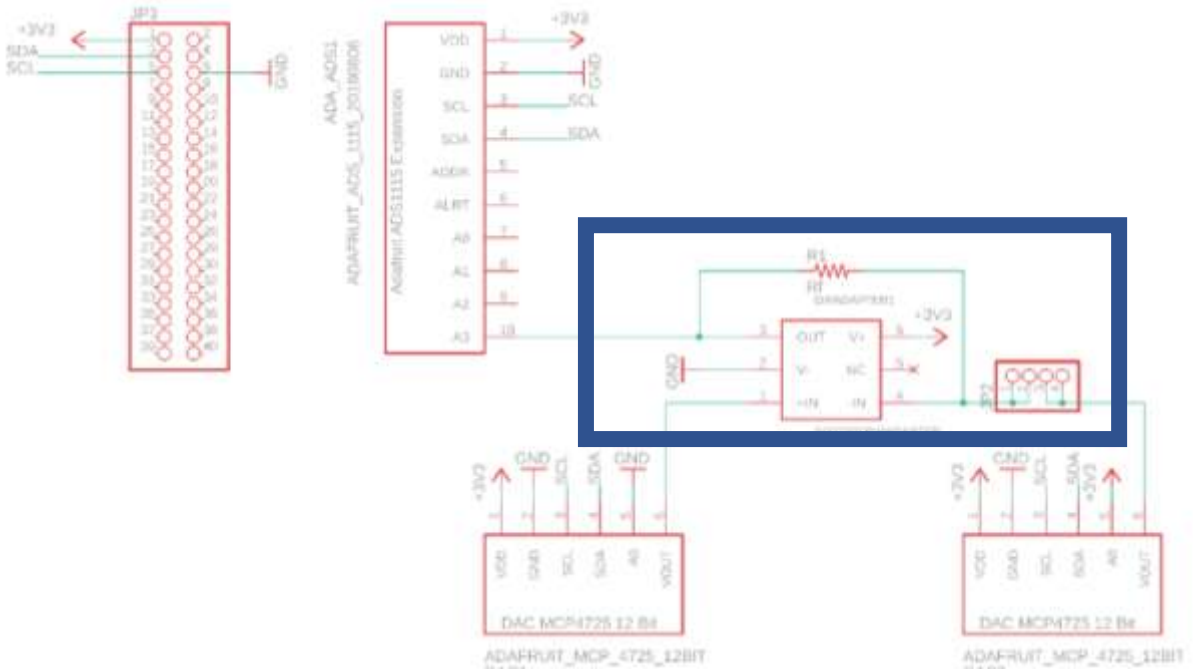

Fig. 3.10: Schematic of the expansion board. The transimpedance amplifier circuit is enclosed in the blue line.

Next, we discuss how the expansion board enabled us to measure I_{ds}. We selected the ADS1115 16-Bit ADC to measure the change of I_{ds}. The ADS1115 is an analog to digital converter that measures the change in voltage at a 16-bit precision for a voltage range between 0 V and 3.3 V [33]. Thus, the theoretical voltage resolution of the device, R_v, which is defined here as the smallest measurable change of voltage, is calculated using the following equation:

$$\mathrm{R_V} = \frac{3.3\ \mathrm{V} - 0\ \mathrm{V}}{2^{16}} = 50\ \mu\mathrm{V}$$

We verified the ADC's performance by testing it and calibrating it using the SPA. We supplied voltages from 0 V to 3.3 V at a step size of 0.5 mV from the SPA to the ADC's measurement pin, A0, and recorded the measured voltage. The resolution achieved was:

$$R_V = 125\ \mu V$$

To determine the RMS fluctuation of the ADC, ΔV, we used the following equation:

$$\Delta V = \frac{1}{P}\sum_{p=0}^{P}\left(\sqrt{\frac{1}{N}\sum_{n=1}^{N}\{(V)_n - \overline{V}\}^2}\right)_p = 50\ \mu V$$

where, N=10, is the total number of measurements for a fixed voltage and, P=6600, is the total number of fixed voltages we supplied from the SPA to the ADS1115.

The ADC is only capable of measuring voltage signals [33]. We measured I_{ds} by converting the current and amplifying it using a transimpedance amplifier circuit. Fig. 3.11 is an illustration of the transimpedance amplifier we built that is part of the expansion board and is illustrated in a blue box in Fig. 3.10. We selected the operational amplifier (OPA) LPV821 for our transimpedance amplifier circuit. The OPA is a low power low-drift amplifier that can be used to measure currents as low as ~1 pA [34]. In Fig. 3.11, the input resistance, R_{in}, acts as the ISFET sensor. The value of R_{in} varies depending on the concentration of the analyte the sensor is placed in. In Fig. 3.11, R_{in} is replaced with four male headers which are used to connect to the ISFET sensor.

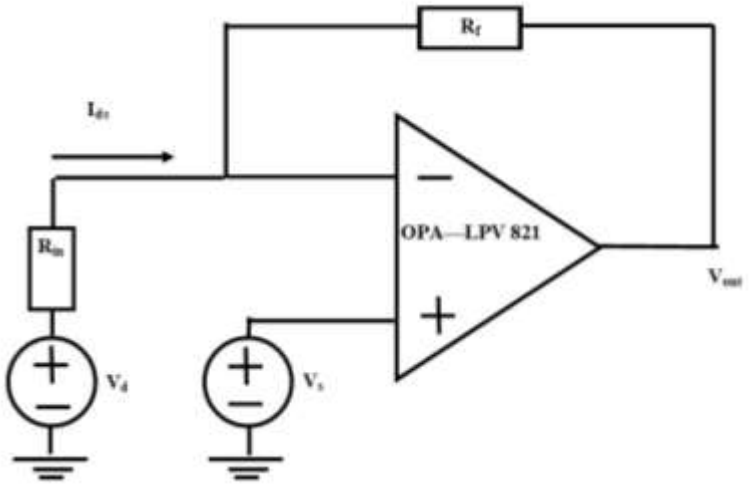

Fig. 3.11: An illustration of the transimpedance amplifier circuit.

In the transimpedance amplifier circuit, I_{ds} is transformed to a voltage, V_{out}, using the following formula:

$$I_{ds} = -\frac{V_{out} - V_s}{R_f}$$

As demonstrated in chapter 2, I_{ds} ranges from ~40µA to ~150µA. We designed the transimpedance amplifier circuit to function for an I_{ds} range of ~0µA to ~250µA using the following two equations:

$$I_{ds-min} = -\frac{V_{out-max} - V_s}{R_f}$$

$$I_{ds-max} = -\frac{V_{out-min} - V_s}{R_f}$$

We then divided the last two equation to get:

$$\frac{I_{ds-min}}{I_{ds-max}} = \frac{\frac{V_{out-max} - V_s}{R_f}}{\frac{V_{out-min} - V_s}{R_f}}$$

We substitute the values in the equation and solve for V_s :

$$\frac{0\ \mu A}{250\ \mu A} = \frac{\frac{0\ V - V_s}{R_f}}{\frac{3.3\ V - V_s}{R_f}}$$

$$V_s = 3.3\ V$$

In chapter 2, we stated that V_{ds} = 0.1 V. Thus, to calculate V_d we used the following equations:

$$V_{ds} = V_d - V_s$$

$$0.1 = 3.3\ V - V_d$$

$$V_d = 3.2\ V$$

To determine the value of the feedback resistance, R_f, we used the following equations:

$$I_{ds} = -\frac{V_{out} - V_s}{R_f}$$

$$250\mu A = -\frac{0 - 3.3V}{R_f}$$

$$R_f = 13.2\ k\Omega$$

The R_f resistor we selected has a resistance of 12.974 kΩ.

The SBC is not capable of supplying analog voltages that are required to bias the graphene ISFET, consequently we used two MCP 4725-12bit DACs as illustrated in Fig. 3.9 and Fig. 3.10. The DAC

is a low-power, high accuracy, single channel, 12-bit buffered voltage output DAC for a voltage range between 0 V and 3.3 V [35]. Thus, the theoretical voltage resolution of the device, R_v, which is defined here as the smallest measurable change of output voltage, is calculated using the following equation:

$$R_V = \frac{3.3\ V - 0\ V}{2^{14}} = 0.806\ mV$$

We verified the DAC's performance by testing it and calibrating it using the SPA. We supplied voltages from the DAC and measured it using the SPA. More specifically, we set the DAC's output pin from 0 to 4095 (2^{14}-1) decimal digits at a step size of one, which corresponds to the voltage range of 0 V to 3.3 V. We achieved a resolution that is equivalent to the theoretical value. Finally, we were required to set V_{ds} to 0.100 V but for our experiment, V_{ds}= 0.1015 V due to the limited resolution of the DAC.

After soldering, the female pin headers, the ADC, the DACs, the OPA, the R_f, and a 1 x 4 male headers onto the PCB, we tested and configured the expansion board. We calibrated the expansion board by mounting it on top of the SBC, as illustrated in Fig. 3.7, and we ran a Python script (presented in the Appendix- section 6.2) that instructs the board to supply V_{ds}=0.1015 V and measure V_{out} which is a function of I_{ds}. We then varied the resistance connected to the male pin headers from ~400 Ω to ~2600 Ω. From this experiment, we generated the calibration equation:

$$I_{ds} = -82.91 * V_{out} + 262.20\ \mu A$$

The calibration curve, for the equation, is illustrated in Fig. 3.12. We also determined the RMS fluctuation seen by the ADS measurement pin, ΔV_{out}, using the following equation:

$$\Delta V_{out} = \frac{1}{P}\sum_{p=0}^{P}\left(\sqrt{\frac{1}{N}\sum_{n=1}^{10}\{(V)_n - \overline{V}\}^2}\right)_p = 0.0012\ V$$

where, N=100, is the total number of measurements of V_{out} for a fixed R_{in} and, P=20, is the total number of R_{in} resistor values we used for calibration. We also calculated the RMS fluctuation in terms of I_{ds}, ΔI_{ds}, using the slope of the calibration equation:

$$\Delta I_{ds} = \Delta V_{out} * |-82.91| \Delta I_{ds} = 0.0012\ V * 82.91 = 0.10\ \mu A$$

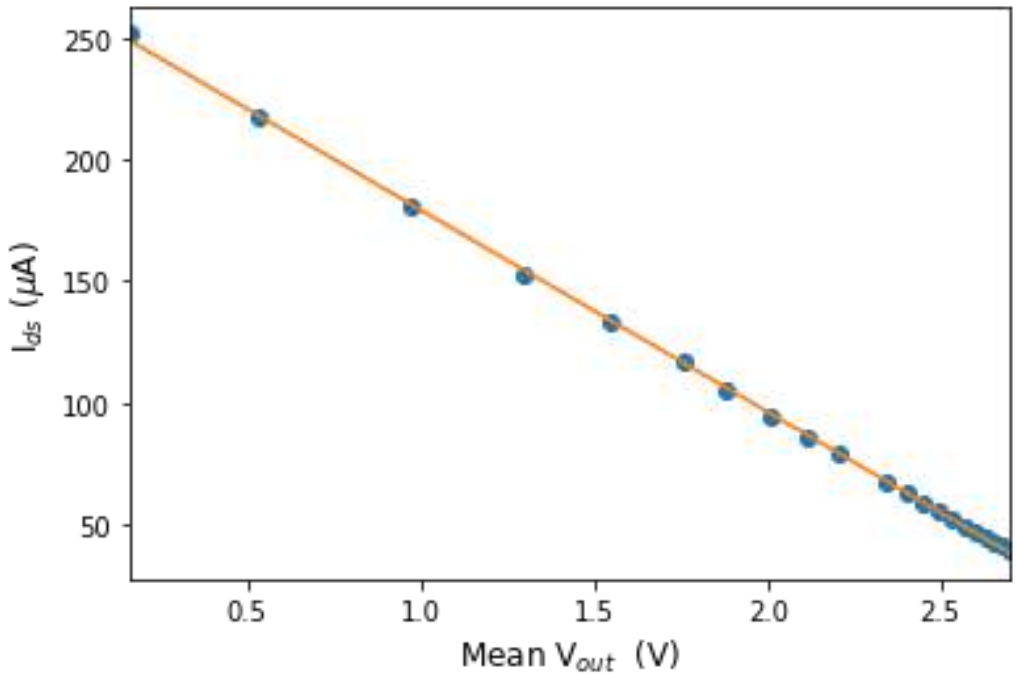

Fig. 3.12: Calibration curve of the expansion board; I_{ds} versus mean V_{out} as we increased the resistance of R_{in} from ~400 Ω to ~2600 Ω.
Calibration equation: $\mathbf{I_{ds}}$ = - 82.91* $\mathbf{V_{out}}$ + 262.2 µA
$\mathbf{\Delta I_{ds}}$: 0.10 µA $\mathbf{\Delta V_{out}}$: 1.2 mV

After we calibrated the expansion board, we connected a ribbon cable from the 3 male pin headers on the expansion board, as illustrated in Fig. 3.13, that terminates at the ISFET sensor case, as illustrated in Fig. 3.14a-c. The ribbon cable is connected such that $V_d = V_{ref} = 3.3$ V and $V_s = 3.2$ V. The ISFET sensor case holds the ISFET sensor and reference electrode so they remain intact when they are submersed in the analyte and prevents any liquid from contacting the wires. The ISFET sensor case is sealed from the front side as illustrated in Fig. 3.14c.

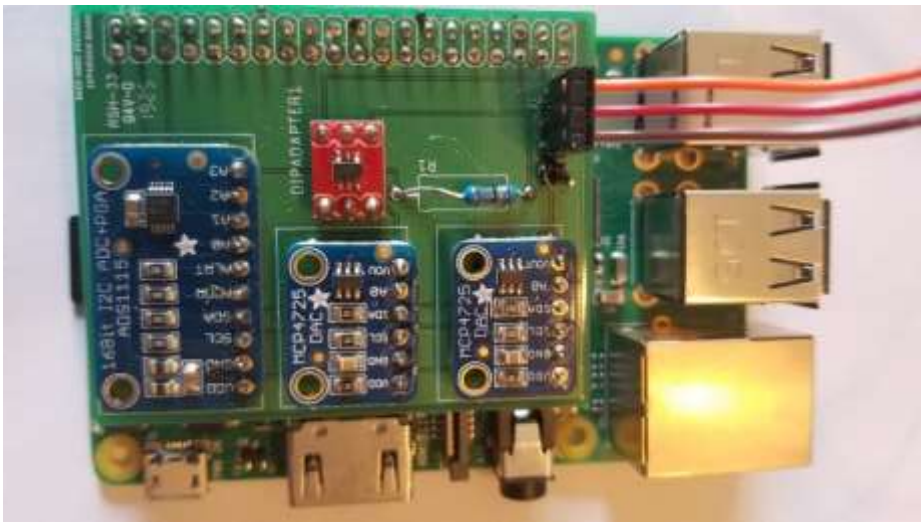

Fig. 3.13: Interrogation circuit with a ribbon cable that terminates at the graphene ISFET holder.

We manufactured the ISFET sensor case, illustrated in Fig. 3.14a-c, from polylactic acid (PLA) plastic via 3D printing. We used PLA because the material is low cost and does not react with the analyte molar concentration levels we tested for. The detailed 3D schematics are illustrated in the Appendix-section 6.3.

(a) (b) (c)

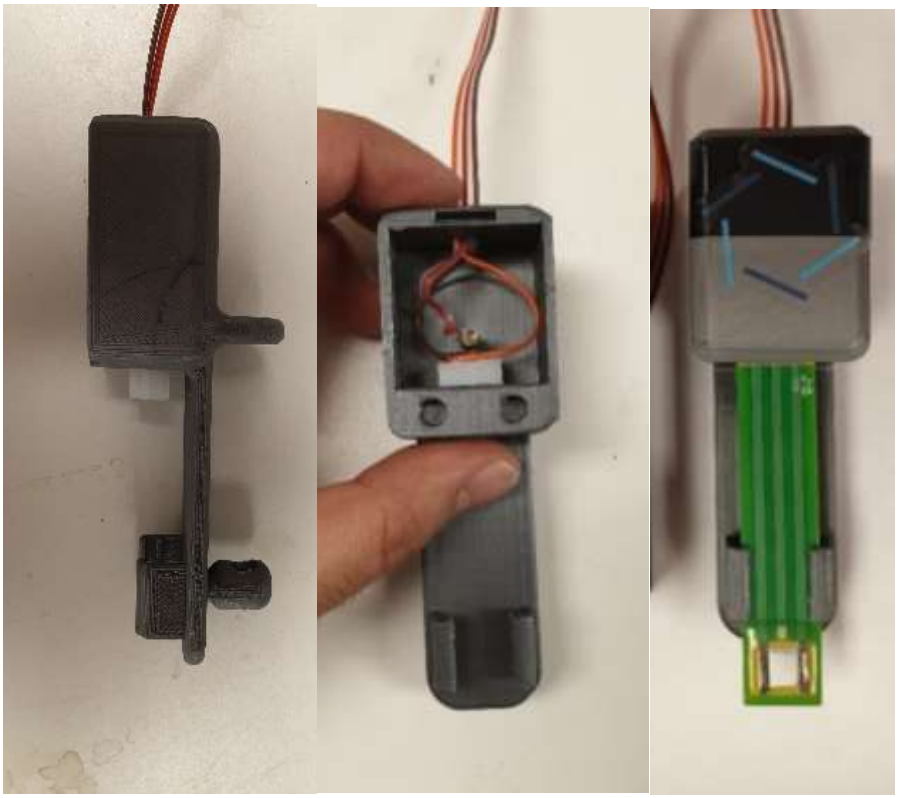

Fig. 3.14: (a) Front view of ISFET sensor case with the wires distribution **(b)** Side view of ISFET sensor case **(c)** Front view of ISFET sensor case after sealing the case with an ISFET sensor connected to it.

In the next chapter, we summarize the setup and results for calibrating and measuring the molar concentration of three ISFET sensors to target K^+, Na^+, and NH_4^+ ions in a solution using the portable device.

4. Molar Concentration Measurements via Portable Device

4.1 Introduction

In this chapter, we summarize the calibration process and present the measurement results of three ISFET sensors to target K^+, Na^+, and NH_4^+ ions in a solution using the portable device. We developed a Python script (presented in the Appendix-section 6.2) to calibrate each ISFET sensor that is sensitive to the ion in question. In this script, we set the voltages that we wanted the interrogation circuit to apply as follows: V_d = 3.3 V, V_s=3.2 V, and V_{ref} = 3.3 V. We also set the number of measurements we wanted to take for a fixed molar concentration to 90 measurements and we set the time between each measurement to 0.5 s. Lastly, we entered the calibration equation from Chapter 3, $\mathrm{I_{ds}} = -82.91 * \mathrm{V_{out}} + 262.20\ \mu\mathrm{A}$, to convert the voltage reading by the ADC to current. The portable device was operated from a laptop, via SSH, and the measurements were stored locally and posted on the IoT platform https://thingspeak.com/ via hypertext transfer protocol (http) requests and using the platform's application programming interface (API) in real-time.

In Chapter 2, we presented the experimental setup using an SPA, which is illustrated in Fig. 2.2. In this chapter, we present a similar setup where we substitute the SPA with the portable device. Fig 4.1 illustrates the experimental setup using the portable device. In our experiment, we began our measurement of I_{ds} with DI water and increased the molar concentration of analyte in a logarithmic fashion with half decade steps (increase in concentration by a factor $10^{0.5}$ for each

step) every ~3 minutes until the analyte reached a molar concentration of 10^{-2} M. Increasing the molar concentration of the analyte was done by adding the proper concentration and volume of stock solution. The steps of preparing stock solution are illustrated in chapter 2. We created a MATLAB script (presented in Appendix-section 6.1) to calculate the volume of stock solution required for a given initial analyte molar concentration and volume, the desired molar concentration, and the stock solution molar concentration. Table 4.1 illustrates the initial volume and molar concentration of the analyte, the volume and molar concentration of the added solution, and the final molar concentration of the analyte after adding the stock solution in our experiment.

We increased the ion concentration of the analyte gradually by adding a higher concentration solution to it (this process is referred to as "spiking" the analyte). As the analyte is being spiked, we measured the I_{ds} of the sensor versus time. We then generated a series of I_{ds} versus time curves and I_{ds} versus molar concentration curves to extract the calibration equation that correlates I_{ds} to the molar concentration, detection limit, sensitivity, resolution, I_{ds} RMS fluctuation and I_{ds} range for each sensor. We present our results and discuss them in the next section. We also, present the results of a live demo that we conducted on-site and in real-time where we varied the molar concentration of the analyte and post the measurements on the IoT platform.

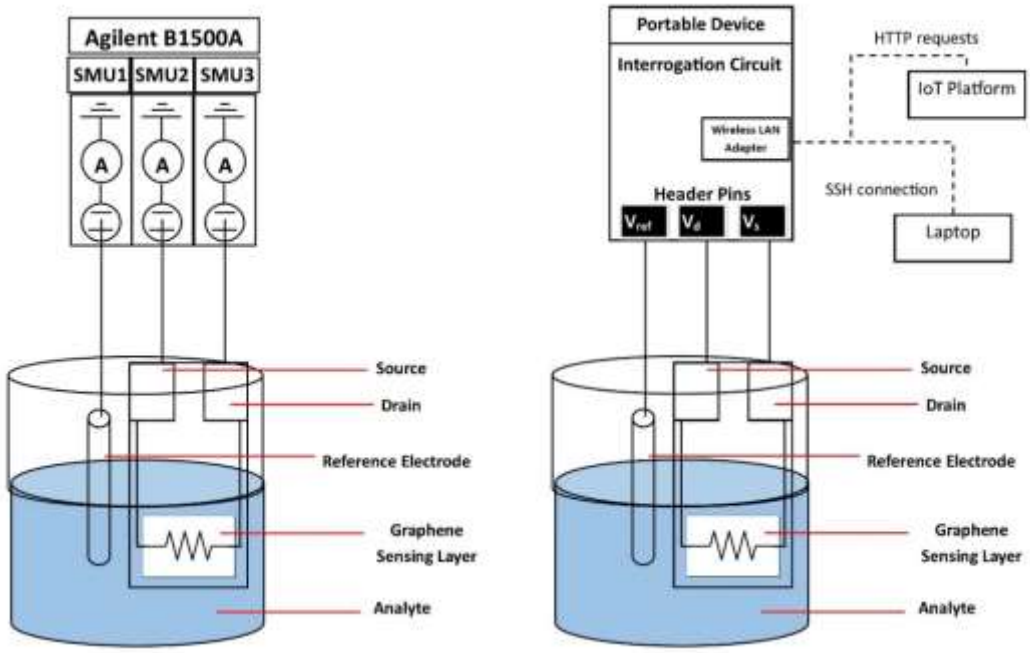

Fig. 4.1: (a) An illustration of the connections of the SPA (Agilent B1500A) to the ISFET sensor and reference electrode in the analyte. (b) An illustration of the connections from the interrogation circuit to the ISFET sensor and reference electrode in the analyte. The wireless connections to the IoT platform and laptop are also presented via the wireless LAN adapter.

Sample Number	Initial Volume of Analyte (µL)	Initial Molar Concentration of Analyte (log(M))	Added Volume of stock solution (µL)	Added Stock solution Concentration (log(M))	Final Molar Concentration of Analyte (log(M))
1	45000	DI water	140	-4	-6.5
2	45140	-6.5	310	-4	-6.0
3	45450	-6.0	1015	-4	-5.5
4	46465	-5.5	3530	-4	-5.0
5	49995	-5.0	110	-2	-4.5
6	50105	-4.5	345	-2	-4.0
7	50450	-4.0	1120	-2	-3.5
8	51570	-3.5	3890	-2	-3.0
9	55460	-3.0	120	0	-2.5
10	55580	-2.5	380	0	-2.0

Table 4.1: The initial volume and molar concentration of the analyte, the volume and molar concentration of the added stock solution, and the final molar concentration of the analyte after adding the stock solution for the portable device.

4.2 Results and Discussion

In this section, we present and discuss our results for measuring I_{ds} as the molar concentration of the analyte is increased using the portable device and we report the results of a demo we conducted on-site and in real-time. Fig. 4.2a-c illustrate our measurements of I_{ds} versus time as we increased the molar concentration of the analytes KCl, NaCl, and NH_4Cl, respectively. We began our measurment with a concetration of -6.5 log(M) and increased it to -2 log(M) in a logarithmic fashion with half decade steps (increase in concentration by a factor $10^{0.5}$ for each step).

(a)

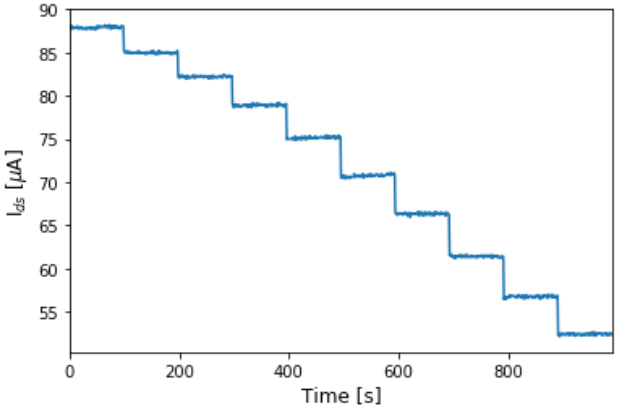

(b)

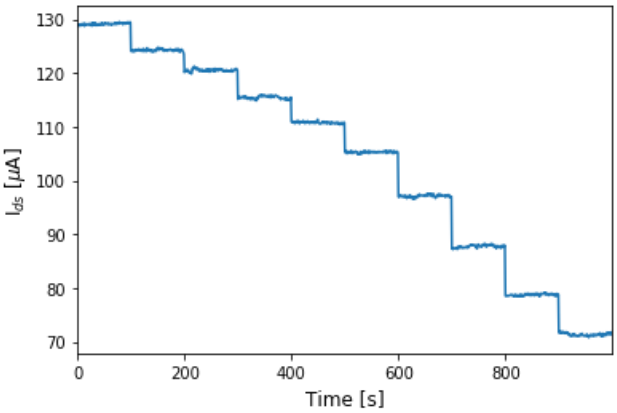

(c)

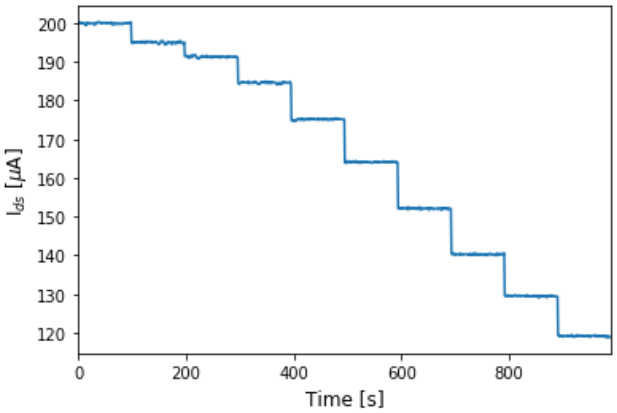

Fig. 4.2: I_{ds} versus time of the (a) K^+ (b) Na^+ (c) NH_4^+ sensitive ISFET as the molar concentration of the analyte is increased from -6.5 to -2 log(M).

From Fig. 4.2a-c we generated Fig. 4.3a-c that illustrates the mean I_{ds} versus molar concentration of each analyte in a logarithmic scale for KCl, NaCl, and NH_4Cl, respectively. From the data presented in Fig. 4.3a-c we extract the sensitivity, detection limit, and resolution of each ISFET sensor and present them in Table 4.2. We also present the I_{ds} RMS fluctuation (ΔI_{ds}) and the I_{ds} range ($I_{ds\text{-}range}$) for each graphene ISFET using the data from Fig. 4.3a-c. The evaluation metrics are defined in Table 2.4.

(a)

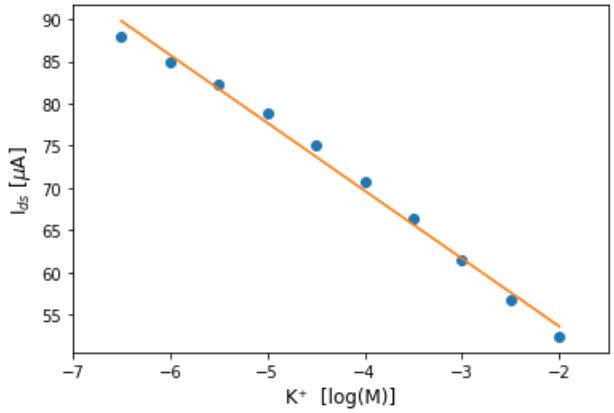

(b)

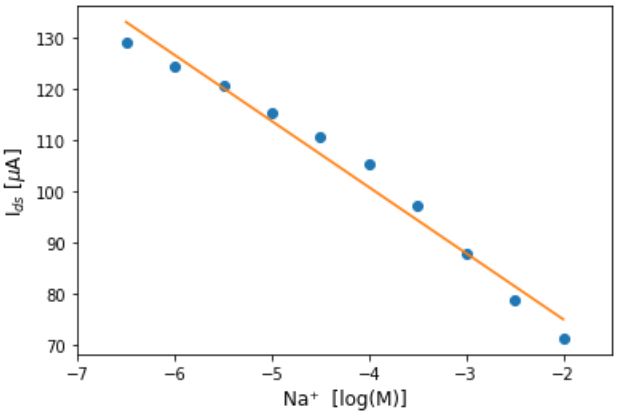

(c)

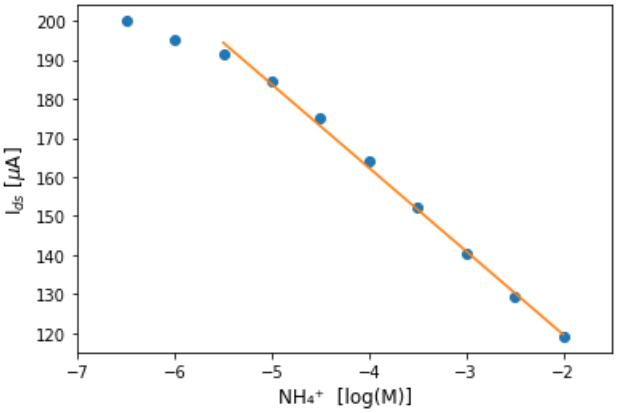

Fig. 4.3: I_{ds} of the (a) K^+ (b) Na^+ (c) NH_4^+ sensitive ISFET versus log(molar concentration) of each graphene ISFET as we increased the concentration of the analyte by half-decades, from -6.5 to -2 log(M).

(a) **S:** -21.36 µA/dec **ΔI_{ds}**: 76.93 µA (b) **S:** -12.89 µA/dec **ΔI_{ds}**: 49.26 µA (c) **S:** -8.043 µA/dec **ΔI_{ds}**: 37.51 µA

ISFET sensor ion detection	Detection limit (log(M))	Sensitivity, S (μA/decade)	I_{ds} RMS fluctuation, ΔI_{ds} (μA)	Resolution, R (Log(M))	$I_{ds\text{-}range}$ (μA)*
K^+	-6.5	-8.04	0.11	0.014	87.94-52.41
Na^+	-6.5	-12.89	0.17	0.013	129.14-71.34
NH_4^+	-5.5	-21.36	0.13	0.0061	199.95- 119.16

Table 4.2: The evaluation metrics; detection limit, sensitivity, I_{ds} RMS-fluctuation, resolution, and mean I_{ds} range for K^+, Na^+, and NH_4^+ sensitive ISFET sensors using the portable device.
* $I_{ds\text{-}range}$ is for the log molar concentration range of -6.5 to -2 log(M).

ISFET sensor ion detection	Detection limit (log(M))	Sensitivity, *S* (μA/decade)	ΔI_{ds} (μA)	Resolution, R (Log(M))	$I_{ds\text{-}range}$ (μA)*
K^+	-5.5	-14.54	0.04	0.002	138.52- 69.38
Na^+	-4	-8.01	0.14	0.017	132.81 - 106.5
NH_4^+	-5	-11.92	0.10	0.0084	139.58 – 91.41

Table 4.3: The evaluation metrics; detection limit, sensitivity, I_{ds} RMS-fluctuation, resolution, and mean I_{ds} range for K^+, Na^+, and NH_4^+ sensitive ISFET sensors using the SPA. This table is identical to Table 2.3.
* $I_{ds\text{-}range}$ is for the log molar concentration range of -7 to -1 log(M).

We present table 4.2 and table 4.3 to compare the performance of the portable device to the SPA in terms of the evaluation metrics. Note that, Table 4.3 is identical to Table 2.3, we present it here again to make it easier for the reader to follow. The detection limit of the portable device exceeds the detection limit of the SPA and there are variations in the sensitivity and $I_{ds\text{-}range}$ between the portable device and the SPA. This behavior is inherent to the ISFET sensors. More specifically, we conducted our measurements using the SPA approximately six months prior to conducting the measurements using the portable device. The ISFET sensors behavior during this time period are likely to have drifted, resulting in drift of the evaluation metrics. The physical origin of long-term drift is not fully understood and remains an active subject of research. However, the SPA has an ΔI_{ds} that is lower than the ΔI_{ds} of the portable device by less than a factor of three, and in one case the resolution agrees to within 21% between device and SPA

interrogated operation. Hence, the design of the portable device has minimized the I_{ds} measurement fluctuation to a comparable level to the SPA.

In Table 4.4, we illustrate the I_{ds} to log molar concentration calibration equation for each graphene ISFET. The calibration equations for each ISFET sensor were extracted from a line of best fit (LOBF) as illustrated in Fig. 4.3a, Fig. 4.4, and Fig.4.3c that target K^+, Na^+, and NH_4^+ ion, respectively. We did not use the LOBF in Fig 4.3b because there is a non-negligible curvature for this ISFET sensor for reasons that we do not yet fully understand, but the systemic curvature is reproducible and stable. Consequently, the sensitivity and resolution do vary with the concentration, so we analyzed the response with a second order polynomial as shown in created Fig. 4.4.

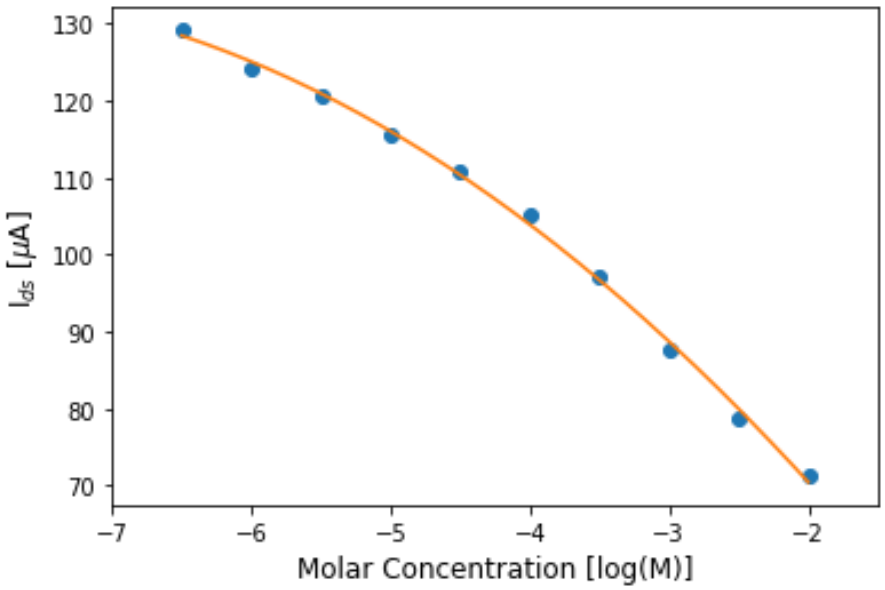

Fig. 4.4: The I_{ds} of the Na^+ sensitive graphene ISFET versus log molar concentration of NaCl as we increased the concentration of the analyte by half-decades, from $10^{-6.5}$ M to 10^{-2} M. The LOBF is a a second order polynomial equation.

ISFET sensor ion detection	Calibration Equation
K^+	**log(M)** = -0.0007111($\mathbf{I_{ds}}$) - 3.285
Na^+	**log(M)** = -0.0007111($\mathbf{I_{ds}}$)^2 + 0.06711($\mathbf{I_{ds}}$) - 3.285
NH_4^+	**log(M)** = -0.0007111($\mathbf{I_{ds}}$) + 3.285

Table 4.4: The calibration equations for K^+, Na^+, and NH_4^+ sensitive ISFET sensors

We incorporated the calibration equations from Table 4.4 into a Python script (presented in Appendix-section 6.2) that converts the I_{ds} measurements to the log molar concentration of each ISFET sensor. The script also posts the data collected to the IoT platform in real-time.

Finally, Fig. 4.6 is a screenshot of the interactive dashboard that displays a graph of the log molar concentration versus time, and a numerical display of the most recent log molar concentration measurement of each graphene ISFET from the demo. This experiment was conducted as a live demonstration for Ericsson at their office in Ville Saint Laurent, Quebec, Canada. These were experiments conducted outside of a controlled laboratory environment, in a conference room. Fundamentally, we demonstrated the capability of our portable device and graphene ISFETs to measure the molar concentration of the analyte in real-time using our IoT platform.

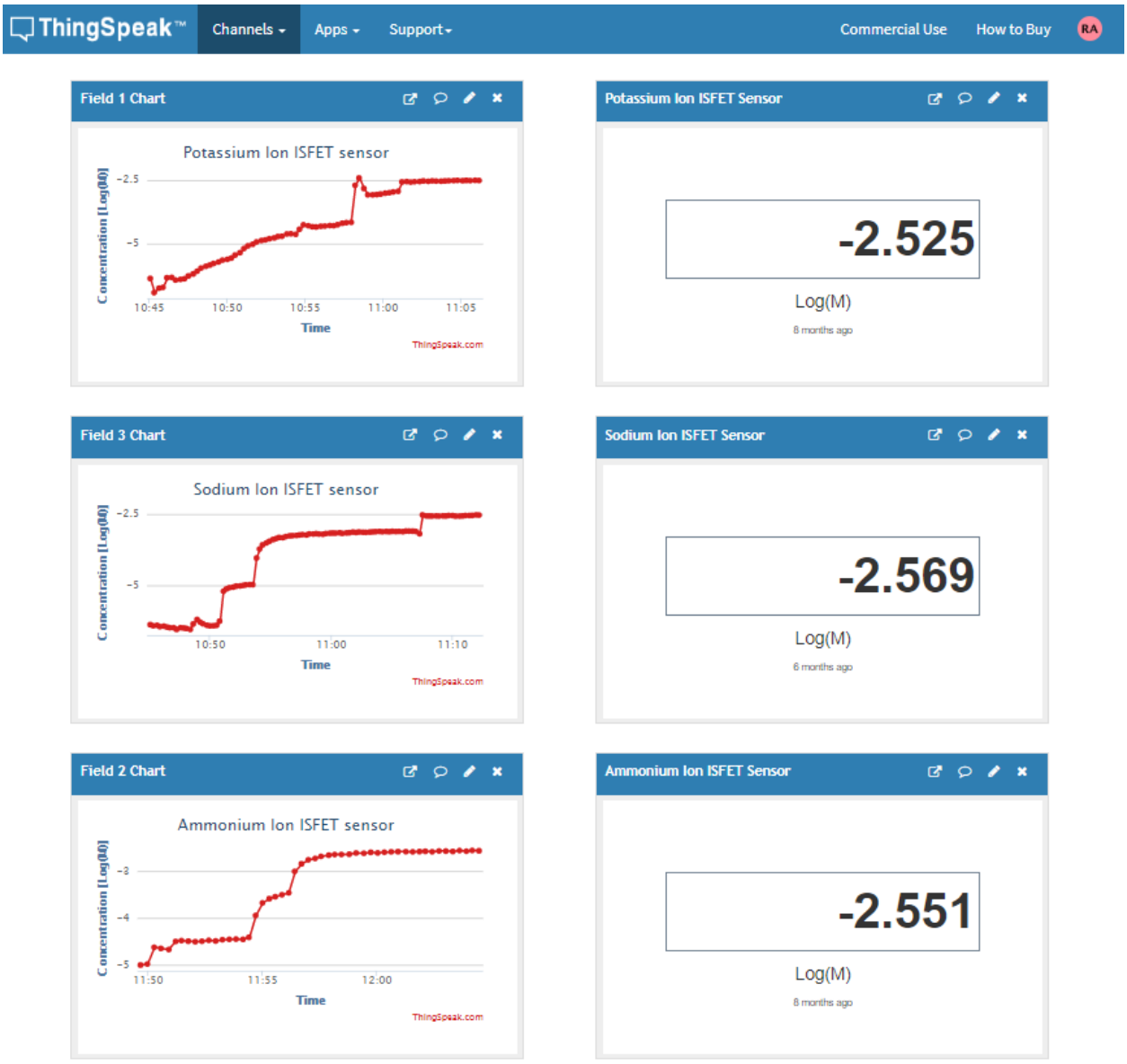

Fig. 4.5: A screenshot of the interactive dashboard on the IoT platform https://thingspeak.com/. On the right side, the log molar concentration versus time plot is displayed for each graphene ISFET. On the left side, a numerical display of the most recent log molar concentration measurement is displayed for each graphene ISFET. The data displayed are measurements conducted in real-time and on-site using the portable device at the Ericsson office in Ville Saint Laurent, Quebec, Canada.

In the next chapter, we summarize the findings and results of this thesis and we discuss potential areas for improvement and further development.

5. Conclusion and Future work

5.1 Conclusion

In this thesis, we presented the portable device that we built as on-site alternative to the SPA to measure the molar concentration of an ion in a solution using graphene ISFETs. The graphene ISEFTs we used target K^+, Na^+, and NH_4^+ ions in solution. They were operated by biasing their drain and source terminals such that V_{ds} = 0.100 V and by biasing the reference electrode such that $V_{ref} = V_d$ while we measured I_{ds}.

We calibrated the graphene ISFETs, using the SPA and the portable device, by increasing the ion concentration of the analyte gradually and we recorded the I_{ds} to establish a relationship between I_{ds} and the molar concentration. We then generated a graph that shows the relationship between I_{ds} and time as the molar concentration increases and we generated a graph that shows the mean I_{ds} versus the log molar concentration for each graphene ISFET. We extracted the evaluation metrics; the detection limit, sensitivity, I_{ds} RMS-fluctuation, resolution, and mean I_{ds} range from these data sets.

We discovered that the SPA has a ΔI_{ds} that is lower than the ΔI_{ds} of the portable device by less than a factor of three, and in some cases differing by only 21%. Hence, the design of the portable device has minimized the I_{ds} measurement fluctuation to a comparable level to the SPA. However, the results of the detection limit, sensitivity, I_{ds} range, and resolution are somewhat inconclusive with the variation between the SPA and the portable device potentially due to drift in the

graphene ISFET characteristics. We conducted our measurements using the SPA approximately six months prior to conducting the measurements using the portable device.

The portable device we built is a compact and integrated solution that includes an interrogation circuit to measure and supply voltages/currents to an ISFET sensor, a case that holds the interrogation circuit, and a case that holds the ISFET sensor and reference electrode. The interrogation circuit is made up of a control board and expansion board. The expansion board realizes functionality that the SBC cannot achieve that are required for our experiments. The interrogation circuit was operated through the SBC via SSH connection from any smart device such as a smart phone or laptop. Finally, the portable device was incorporated into an online IoT platform called ThingSpeak (https://thingspeak.com/). This platform allowed us to collect, visualize, and analyze live data streams of the measured molar concentration from different graphene ISFETs. We demonstrated this capability in real-time and on-site using the portable device at the Ericsson office in Ville Saint Laurent, Quebec, Canada.

5.2 Future work

There are three main areas that are open for improvement and further development including: the graphene ISFETs, the portable device, and the IoT platform.

From our experiments, we discovered that the graphene ISFETs had a potentially unstable behavior that resulted in inconclusive the evaluation metrics. The sensitivity, detection limit, resolution, and I_{ds} range for each graphene ISFET showed variations when we calibrated them using the SPA and the portable device. While the developing the graphene ISFETs was outside the scope of this thesis, there remains a need to understand the origin of and thereby improve the reliability and stability of the graphene ISFETs This will contribute to reliable on-site and real-time measurements For the scope of this thesis, we limited our experiment to graphene ISFETs that are sensitive to K^+, Na^+, NH_4^+ ions primarily because they are the most reliable ISFETs available to us. We should explore the feasibility of developing graphene ISFETs that are sensitive to ions that are critical for water quality monitoring applications such as H^+ [36]. Furthermore, ion concentrations are insufficiently measured in both space and time even in developed countries such as Canada. Across Canada, there are only 19 sites that continuously monitor water quality of water ways, such as rivers and lakes, with automated water quality monitoring systems [36]. In Quebec, to monitor the 500 km long St. Lawrence river, water samples are taken to labs from 10 different locations once every few weeks to be measured by either chromatography or spectroscopy [37]. Fig. 5.1 is a map of the St. Lawrence river with the locations of the water collection sites for water quality monitoring. By adding more graphene ISFETs that are sensitive to ions that are relevant for water quality monitoring applications we can enable the possibly of monitoring water quality in real-time and on-site. Nevertheless, the graphene ISFETs must be

tested under the physical conditions of the external environment, that includes extreme temperatures and bio flawing ensure reliable functionality.

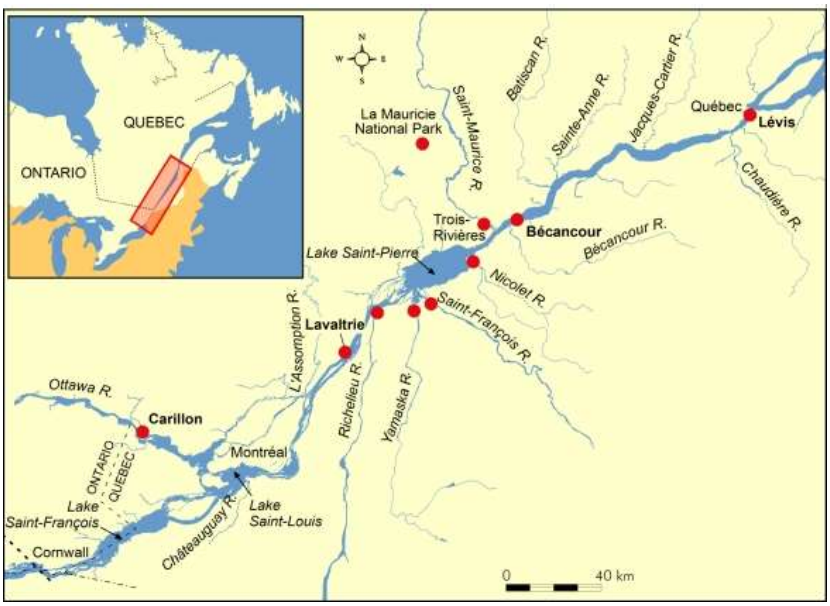

Fig. 5.1: A map of the St. Lawrence river. The red dots are the 10 locations water is collected from to conduct water quality assessment [37].

The portable device has several areas of improvement that are primarily the interrogation circuit and its case. Regarding the interrogation circuit, we can develop a more efficient and compact design. The control board we selected for our portable device is the Raspberry Pi 3- Model B. More compact models are available with the same functionality as the Raspberry Pi 3- Model B. For example, the Raspberry Pi Zero W is a smaller size board. Fig. 5.2 shows a picture of the Raspberry Pi 3 (on the right side) and Raspberry Pi Zero W (on the left side) to show the size of the two boards. The Raspberry Pi Zero W also requires less power than the Raspberry Pi 3- Model B. More specifically, the Raspberry Pi Zero W consumes ~0.4 W of power while the Raspberry Pi 3- Model B consumes ~1.2-1.4 W of power [38]. Furthermore, we can explore the feasibility of the replacing the SBC with a microcontroller because microcontrollers tend to be cheaper and

can fulfil the same functionality required for the portable device. The main difference between an SBC and a microcontroller is that an SBC runs on an operating system. This is important because we can program an SBC with a higher-level programming language such as Python while a microcontroller requires a lower level language such as C, and thus the microcontroller requires more custom programming. However, the simplicity of the SBC approach comes at the expense of large size, higher cost, and higher energy consumption [39], [40].

Fig. 5.2: On the right we present the Raspberry Pi 3 and on the left we present the Raspberry Pi Zero W [41].

The expansion board can also be improved to reduce the size of the expansion board, reduce the I_{ds} RMS fluctuation of the I_{ds} measurement, and increase the functionality of the expansion board. All the components on our expansion board are through hole devices. We can replace these components with surface mount devices, which are smaller, to make the expansion board smaller or to provide space to increase or improve the functionality of the expansion board. For example, the I_{ds} RMS fluctuation of our interrogation circuit is almost three times higher as compared to the SPA for one of our graphene ISFETs. We can add noise filtering components, such as an RC circuit, to reduce the noise and as a result potentially reduce the I_{ds} RMS fluctuation. We did not explore adding noise filtering components to the expansion board due to space limitations. Also,

we can explore using a higher resolution ADC to increase the resolution of our I_{ds} measurements. For example, another option is the MCP3424 18-Bit ADC [42], which has a resolution that is 2 bits higher than the ADS1115 used in our current work. We could not use the MCP3424 ADC for our expansion board because it is slightly larger than the ADS1115 [42], [43]. Finally, we could use the additional space to add to the functionality of our expansion board. For example, we can explore the possibility of increasing the number of graphene ISFETs that the portable device operates simultaneously. The ADS1115 has four voltage measuring channels which allows us to operate up to four graphene ISFETs simultaneously. This can be achieved by simply adding three transimpedance amplifier circuits that connect the graphene ISFETs to the voltage measuring channels of the ADS1115. We can also explore the feasibility of developing a completely new design for the interrogation circuit that allows us to operate more than four graphene ISFETs simultaneously.

The case we developed for the interrogation circuit was preliminary in nature. For our interrogation circuit, we simply combined two Raspberry Pi 3 cases to create space for the expansion board. However, the case does not offer protection against water or harsh conditions such as high temperature, physical impact, or high relative humidity. It is important to develop a more robust case that encloses the interrogation circuit and the graphene ISFETs such that they can withstand harsh conditions allowing us to conduct on-site measurements in the field such as rivers and lakes.

Lastly, we did not use the IoT platform to its fullest potential. At all times only one portable device was connected to the IoT platform, and the molar concentrations were posted for only one ISFET at any given moment. To fully capitalize on the potential of IoT, we want to post molar

concentration measurements from multiple portable devices from different geographical locations. Also, we can explore alternative IoT platforms that does not restrict us to only posting data but allows us to operate the devices from the IoT platform instead of our current method where we SSH into the portable device from a laptop or smart device.

6. Appendix

6.1 MATLAB Script for Creating Stock Solutions

The MATLAB script illustrated in Fig. A.1 was used to calculate the volume of stock solution required for a given initial analyte molar concentration and volume, the desired molar concentration, and the stock solution molar concentration. These parameters are set in lines 5 to 8.

```
clear all
close all

%set these parameters and run 1e-2
molarityinit = 1*10^(-2.5);
volinitml = 45 + 140e-3 + 310e-3 + 1015e-3 + 3530e-3 +110e-3 +
1120e-3 + 3890e-3 + 120e-3;
addconc = 1e-0;
molaritydesired = 1*10^(-2.0);
%---------------%b

points = 10001;
addvolml = linspace (0,8,points);

for i = 1:points
    concentration(i) =
(addvolml(i)*addconc+molarityinit*volinitml)/(volinitml+addvolml
(i));
    err(i) = abs(concentration(i)-molaritydesired);
end

[n ,m] = min(err);

plot(addvolml,concentration)
xlabel('volume to add (ml)')
ylabel('concentration (M)')
legend(['Volume to add = ' num2str(addvolml(m)*1e3) ' uL'])
```

6.2 Python Scripts for the Portable Device

6.2.1 The Python script that was used to generate the calibration equation of the expansion board. The calibration equation converts the measured I_{ds} to a voltage V_{out}.

```
import time
import smbus2
import csv
import ADS1115_Configuration
import DAC_MCP4725_Configuration
import math as mp
import statistics as st

file_name = '20190706.csv'
SPS = 128
Number_of_samples = 100
DAC_VDD_value = 4096
DAC_GND_value = 3982
Vin_Vs_difference = 100.0  # mV
Vin_Vs_difference_fluctuation = 0.05  # mV
voltages_reading = []
voltage_difference_list = []
Resistor_values = {0:100000000, 1: 2568.8, 2: 2464.5, 3: 2359.7, 4: 2255.2,
                   5: 2150.6, 6: 2045.7, 7: 1935.96, 8: 1826.39,
                   9: 1717.05, 10: 1606.83, 11: 1497.09,
                   12: 1390.46, 13: 1283.27, 14: 1177.16,
                   15: 1070.48, 16: 963.49, 17: 861.80,
                   18: 759.83, 19: 660.09, 20: 560.08, 21: 463.89, 22:401.43, 23: 374.06}

# ADS Initiation
A3_READ = ADS1115_Configuration.ADS1115(pin_selector="A3", SPS=SPS)

# DAC Initiation
# Address 0x62 A1 => GND     # Vs on the board
DAC_GND = DAC_MCP4725_Configuration.MCP4725(address=0x62)
# Address 0x63 A0 => 3.3V    # Vin on the board
DAC_VDD = DAC_MCP4725_Configuration.MCP4725(address=0x63)
```

```
# Setting the DAC voltages; the voltage difference is 100.0 +- 0.05mV
DAC_VDD.set_voltage(DAC_VDD_value, persist=False)
DAC_GND.set_voltage(DAC_GND_value, persist=False)

print('Enter the position of the resistor')
position = int(input())

positions_list = position * Number_of_samples

time.sleep(0.5)

for i in range(0, Number_of_samples):
   reading_A3 = A3_READ.Retrieve_Reading()
   voltages_reading.append(reading_A3)
   print(reading_A3)
   time.sleep(0.5)


mean_voltage = [st.mean(voltages_reading)]* Number_of_samples
diff = map(float.__sub__, voltages_reading, mean_voltage)
MSE = list(map(abs, diff))
average_MSE = st.mean(MSE)


for count, volt in enumerate(voltages_reading):
   with open(file_name, mode='a') as our_data:
      our_data_writer = csv.writer(our_data)
      our_data_writer.writerow([position,count, Resistor_values[position],
voltages_reading[count], mean_voltage[count], MSE[count], average_MSE, SPS,
Number_of_samples])
   our_data.close()
```

6.2.2 The Python script that converts the Ids measurement to the log molar concentration of a graphene ISFET and posts the log molar concentration on the IoT platform in real-time.

```
import time
import csv

# Import the ADS1x15 module.
import Adafruit_ADS1x15
import Adafruit_MCP4725


# Initialize DAC MCP4725 instance
# Create an ADS1115 ADC (16-bit) instance
# Set the gain to 1
adc = Adafruit_ADS1x15.ADS1115()
# top (vs)
dac = Adafruit_MCP4725.MCP4725(address=0x63, busnum=1)
# bottom
dac2 = Adafruit_MCP4725.MCP4725()

GAIN = 1

with open('configuration_voltage_values.csv') as readFile:
   reader = csv.reader(readFile, delimiter = ',')
   lines = list(reader)
   print(lines)
   print(type(lines))
readFile.close()

print(lines[2])

DAC = [[],[],[],[]]
for count, row in enumerate(lines):
   for item in row:
      DAC[count].append(float(item))
print(DAC)

print("Enter Voltages between 0V and 3.3 V")

print("Enter voltages between 0V and 3.3V")
entered_voltage_1 = input()
entered_voltage_2 = input()

entered_voltage = [float(entered_voltage_1), float(entered_voltage_2), 0, 0]
```

```
differences_list = [[],[],[],[]]
positions_of_smallest_difference= []

for count, row in enumerate(DAC):
   for count2, value in enumerate(row):
      differences_list[count].append(abs(value-entered_voltage[count]))
print(differences_list)

for count, row in enumerate(differences_list):
   minpos = row.index(min(row))
   positions_of_smallest_difference.append(minpos)
print(positions_of_smallest_difference)

for i in range(0,2):
   print("The output voltage for DAC" + str(i) + " " +
str(DAC[i][positions_of_smallest_difference[i]]) + " The DAC value is "+
str(positions_of_smallest_difference[i]))

dac.set_voltage(positions_of_smallest_difference[0])
dac2.set_voltage(positions_of_smallest_difference[1])

print('Reading ADS1x15 values, press Ctrl-C to quit...')
# Print nice channel column headers.
print('| {0:>6} | {1:>6} | {2:>6} | {3:>6} |'.format(*range(4)))
print('-' * 37)
# Main loop.


for i in range(0,100):
   # Read all the ADC channel values in a list.
   values = [0]*4
   for i in range(4):
      # Read the specified ADC channel using the previously set gain value.
      values[i] = adc.read_adc(i, gain=GAIN)*0.000125020670961 - 0.000015820602657
      # Note you can also pass in an optional data_rate parameter that controls
      # the ADC conversion time (in samples/second). Each chip has a different
      # set of allowed data rate values, see datasheet Table 9 config register
      # DR bit values.
      #values[i] = adc.read_adc(i, gain=GAIN, data_rate=128)
      # Each value will be a 12 or 16 bit signed integer value depending on the
```

```
    # ADC (ADS1015 = 12-bit, ADS1115 = 16-bit).
  # Print the ADC values.
  print('| {0:>6} | {1:>6} | {2:>6} | {3:>6} |'.format(*values))
  # Pause for half a second.
  time.sleep(0.5)
  with open('voltages_list', mode ='a') as our_data:
    our_data_writer = csv.writer(our_data)
    our_data_writer.writerow(values)
  our_data.close()
```

6.2.3 The Python script that calibrates I_{ds} measurement to the log molar concentration for the graphene ISFETs.

```
import time
import smbus2
import csv
import ADS1115_Configuration
import DAC_MCP4725_Configuration
import math as mp
import statistics as st
import requests
import math

API_ENDPOINT = 'https://api.thingspeak.com/update'
API_KEY = "JYUAJL4M63PZIAF8"

selected_sensor = str(input())

print('we are here!')
file_name = '20190816_01.csv'
file_name_100 = '20190816_01_last100.csv'

SPS = 128
Number_of_samples = 600
DAC_VDD_value = 4096
DAC_GND_value = 3982
Vin_Vs_difference = 100.0  # mV
Vin_Vs_difference_fluctuation = 0.05  # mV
voltages_reading = []
```

```
voltage_difference_list = []
Resistor_values = {0: 100000000, 1: 2568.8, 2: 2464.5, 3: 2359.7, 4: 2255.2,
                   5: 2150.6, 6: 2045.7, 7: 1935.96, 8: 1826.39,
                   9: 1717.05, 10: 1606.83, 11: 1497.09,
                   12: 1390.46, 13: 1283.27, 14: 1177.16,
                   15: 1070.48, 16: 963.49, 17: 861.80,
                   18: 759.83, 19: 660.09, 20: 560.08, 21: 463.89, 22: 401.43, 23: 374.06}

# ADS Initiation
A3_READ = ADS1115_Configuration.ADS1115(pin_selector="A3", SPS=SPS)

# DAC Initiation
# Address 0x62 A1 => GND     # Vs on the board
DAC_GND = DAC_MCP4725_Configuration.MCP4725(address=0x62)
# Address 0x63 A0 => 3.3V    # Vin on the board
DAC_VDD = DAC_MCP4725_Configuration.MCP4725(address=0x63)

# Setting the DAC voltages; the voltage difference is 100.0 +- 0.05mV
DAC_VDD.set_voltage(DAC_VDD_value, persist=False)
DAC_GND.set_voltage(DAC_GND_value, persist=False)

print('Enter the position of the resistor')
position = int(input())

positions_list = position * Number_of_samples

time.sleep(0.5)

# for i in range(0,5):
# time.sleep(60)
# print("Minutes of waiting complete: " + str(i))


for i in range(0, Number_of_samples):
    reading_A3 = A3_READ.Retrieve_Reading()
    voltages_reading.append(reading_A3)
    print(str(i) + ": " + str(reading_A3))

    if selected_sensor == 'K':
        A3_Reading_converted = 0.0000000274 * reading_A3 ** 3 - 0.0001865362 * reading_A3
** 2 + 0.4291380427 * reading_A3 - 337.1473295468
```

```
        data = {'api_key': API_KEY, 'field1': str(round(A3_Reading_converted, 4))}
        r = requests.post(url=API_ENDPOINT, data=data)
        pastebin_url = r.text
    elif selected_sensor == 'Na':
        A3_Reading_converted = 0.0000000497 * reading_A3 ** 3 - 0.0003285990 * reading_A3
** 2 + 0.7286591876 * reading_A3 - 544.9830203054
        data = {'api_key': API_KEY, 'field2': str(round(A3_Reading_converted, 4))}
        r = requests.post(url=API_ENDPOINT, data=data)
        pastebin_url = r.text
    elif selected_sensor == 'NH4':
        A3_Reading_converted = 0.0000000131 * reading_A3 ** 3 - 0.0000516504 * reading_A3
** 2 + 0.0709137793 * reading_A3 - 37.1289390446
        data = {'api_key': API_KEY, 'field3': str(round(A3_Reading_converted, 4))}
        r = requests.post(url=API_ENDPOINT, data=data)
        pastebin_url = r.text
    else:
        print('Sensor does not exist')
    time.sleep(5)

mean_voltage = [st.mean(voltages_reading)] * Number_of_samples
diff = map(float.__sub__, voltages_reading, mean_voltage)
MSE = list(map(abs, diff))
average_MSE = st.mean(MSE)

voltages_reading_last_100 = voltages_reading[500:599]
mean_voltage_last_100 = 100 * [st.mean(voltages_reading_last_100)]
diff_100 = map(float.__sub__, voltages_reading_last_100, mean_voltage_last_100)
MSE_100 = list(map(abs, diff_100))
average_MSE_100 = st.mean(MSE_100)

for count, volt in enumerate(voltages_reading):
    with open(file_name, mode='a') as our_data:
        our_data_writer = csv.writer(our_data)
        our_data_writer.writerow(
            [position, count, voltages_reading[count], mean_voltage[count], MSE[count],
average_MSE])
    our_data.close()

for count, volt in enumerate(voltages_reading_last_100):
    with open(file_name_100, mode='a') as our_data:
        our_data_writer = csv.writer(our_data)
```

```
        our_data_writer.writerow(
            [position, count, voltages_reading_last_100[count], mean_voltage_last_100[count],
MSE_100[count],
             average_MSE_100])
    our_data.close()
print("Complete!")
```

6.3 Schematic of the 3D printed ISFET sensors holder

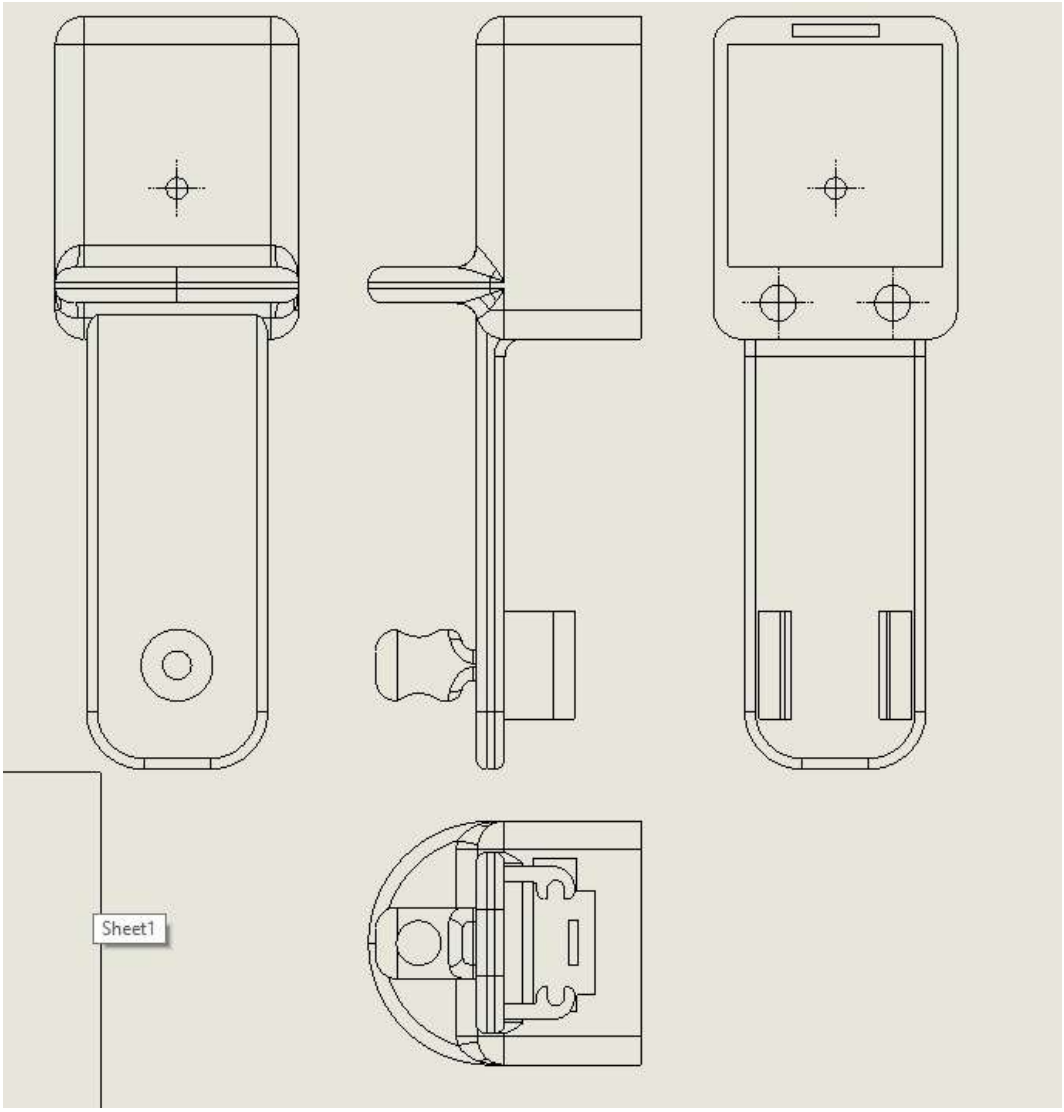

Fig. 6.1: The schematic of the 3D printed ISFET sensors holder.

7. References

[1] Y. Liu, H. Li, G. Cui and Y. Cao, "Water quality attribution and simulation of non-point source pollution load flux in the Hulan River basin," *Scientific Reports,* no. 10, 20 February 2020.

[2] X. Chen, L. Yu, S. Zou, L. Xiao and J. Fan, "Zeolite Cotton in Tube: A Simple Robust Household Water Treatment Filter for Heavy Metal Removal," *Scientific Reports,* vol. 10, 13 March 2020.

[3] S. Redhai, C. Pilgrim, P. Gaspar, L. v. Giesen, T. Lopes, O. Riabinina, T. Grenier, A. Milona, B. Chanana, J. B. Swadling, Y.-F. W. Dahalan, M. Yuan, M. Wilsch-Brauninger, W.-h. Lin and Nat, "An intestinal zinc sensor regulates food intake and developmental growth," *Nature,* vol. 580, p. 263–268, 2020.

[4] R. L. Miller, S. E. Guimond, R. Schwörer, O. V. Zubkova, P. C. Tyler, Y. Xu, J. Liu, P. Chopra, G.-J. Boons, M. Grabarics, C. Manz, J. Hofmann, N. G. Karlsson, J. E. Turnbull and W. Struwe, "Shotgun ion mobility mass spectrometry sequencing of heparan sulfate saccharides," *Naure Communication,* vol. 11, 2020.

[5] N. Amornwichet, T. Oike, A. Shibata, C. Nirodi, H. Ogiwara, H. Makino, Y. Kimura, Y. Hirota, M. Isono, Y. Yoshida, T. Ohno, T. Kohno and T. Nakano, "The EGFR Mutation Status Affects the Relative Biological Effectiveness of Carbon-Ion Beams in Non-Small Cell Lung Carcinoma Cells," *Scientific Reports,* vol. 5, 15 June 2015.

[6] I. Fakih, F. Mahvash, M. Siaj and T. Szkopek, "Sensitive Precise pH Measurement with Large-Area Graphene Field-Effect Transistors," *Phys. Rev. Applied,* vol. 8, 30 October 2017.

[7] A. J. Bard and L. R. Faulkner, Electrochemical Methods: Fundamentals and Applications, New York: John Wiley and Sons, 2001.

[8] B. RAWLING, M. GREAVES and M. AMOS, "Determination of Silver in Lead Concentrates by Atomic Absorption Spectroscopy," *Nature,* no. 188, p. 137–138, 1960.

[9] E. Akbari, R. Moradi, A. Afroozeh, A. Alizadeh and M. Nilashi, "A new approach for prediction of graphene based ISFET using regression tree and neural network," *Superlattices and Microstructures,* vol. 130, pp. 241-248, June 2019.

[10] S. M. Sze and K. K. Ng, Physics of Semiconductor Devices, Hoboken, New Jersey: John Wiley & Sons, Inc., 2007.

[11] J. X. Zhang and K. Hoshino, Molecular Sensors and Nanodevices: Principles, Designs and Applications in Biomedical Engineering, 2nd ed., London: Academic Press, 2019, pp. 181-230.

[12] I. Fakih, A. Centeno, A. Zurutuza, B. Ghaddab, M. Siajc and T. Szkopek, "High resolution potassium sensing with large-area graphene field-effect transistors," *Sensors and Actuators B: Chemical,* vol. 291, pp. 89-95, July 2019.

[13] R. Bhardwaj, S. Majumder, P. K., S. Sinha, R. Sharma, R. Mukhiya and P. Narang, "Temperature compensation of ISFET based pH sensor using artificial neural networks," *IEEE Regional Symposium on Micro and Nanoelectronics,* 2017.

[14] B. Oram, "Ammonia in Groundwater, Runoff, Surface Water, Lakes and Streams," Water Research Center, 2014. [Online]. Available: https://water-research.net/index.php/ammonia-in-groundwater-runoff-and-streams. [Accessed 2 February 2020].

[15] "Do the Nessler and Salicylate methods detect ammonia or ammonium?," Hach Company, 13 06 2019. [Online]. Available: https://frsupport.hach.com/app/answers/answer_view/a_id/1000858/~/do-the-nessler-and-salicylate-methods-detect-ammonia-or-ammonium%3F-. [Accessed 8 February 2020].

[16] U. E. P. Agency, "Drinking Water Advisory: Consumer Acceptability Advice and Health Effects Analysis on Sodium," U.S. Environmental Protection Agency, Washington, DC, 2003.

[17] World Health Organization, "Potassium in drinking-water Background document for development of WHO Guidelines for Drinking-water Quality," WHO Document Production Services, Geneva, Switzerland, 2009.

[18] Agilent B1500A Semiconductor Device Analyzer User's Guide, Santa Clara, California: Agilent Technologies, 2007.

[19] "Raspberry Pi Pinout Diagram | Circuit Notes," Jameco, [Online]. Available: https://www.jameco.com/Jameco/workshop/circuitnotes/raspberry-pi-circuit-note.html. [Accessed 31 05 2020].

[20] J. Sastry, J. Ganesh and J. Bhanu, "I2C based Networking for Implementing Heterogeneous Microcontroller based Distributed Embedded Systems," *Indian Journal of Science and Technology,* vol. 8, no. 15, 2015.

[21] B. Croitoru, A. Tulbure, M. Abrudean and a. M. Secara, "Creating a transducer electronic datasheet using I2C serial EEPROM memory and PIC32-based microcontroller development board," *Proc. SPIE 9258, Advanced Topics in Optoelectronics, Microelectronics, and Nanotechnologies VII,* vol. 9258, 25 February 2015.

[22] M. Maksimović, V. Vujović, N. Davidović, V. Milošević and B. Perišić, "Raspberry Pi as Internet of Things hardware: Performances and Constraints," in *Proceedings of 1st International Conference on Electrical, Electronic and Computing Engineering*, Vrnjačka Banja, 2014.

[23] A. Raza, A. A. Ikram, A. Amin and A. J. Ikram, "A review of low cost and power efficient development boards for IoT applications," in *2016 Future Technologies Conference (FTC)*, San Francisco, CA, 2016.

[24] G. S. Pannu, M. Dawud and P. Gupta, "Design and Implementation of Autonomous Car using Raspberry Pi," *International Journal of Computer Applications,* vol. 113, no. 9, 2015.

[25] "RASPBERRY Pi BASED OBSTACLE AVOIDING ROBOT," *International Research Journal of Engineering and Technology,* vol. 04, no. 02, February 2017.

[26] M. Runia and K. Gagneja, "Raspberry Pi Webserver," in *International Conference on Embedded Systems and Applications (ESA)*, Athens, 2015.

[27] R. Golden, Raspberry Pi Networking Cookbook, Birminghan: Packt Publishing, 2013.

[28] J. Gubbi and R. Buyya, "Internet of Things (IoT): A vision, architectural elements, and future directions," *Future Generation Computer Systems,* vol. 29, no. 7, pp. 1645-1660, 2013.

[29] I. Lee and K. Lee, "The Internet of Things (IoT): Applications, investments, and challenges for enterprises," *Business Horizons,* vol. 58, no. 4, pp. 431-440, 2015.

[30] C. Networks, "The Internet of Things: A survey," *Computer Networks,* vol. 54, no. 15, pp. 2787-2805, 2010.

[31] "RaspberryPI models comparison," Social Compare, 2020. [Online]. Available: https://socialcompare.com/en/comparison/raspberrypi-models-comparison. [Accessed 20 June 2020].

[32] "Smraza Compatible with Raspberry Pi 4 Case, Acrylic Case with 35 x 35 mm Cooling Fan, 4PCS Heatsinks for Raspberry Pi 4 Model B (Upgrade, Large Fan and Large Heat Sinks) - Black," Amazon, 2020. [Online]. Available: Smraza Compatible with Raspberry Pi 4 Case, Acrylic Case with 35 x 35 mm Cooling Fan, 4PCS Heatsinks for Raspberry Pi 4 Model B (Upgrade, Large Fan and Large Heat Sinks) - Black. [Accessed 6 June 2020].

[33] "ADS111x Ultra-Small, Low-Power, I2C-Compatible, 860-SPS, 16-Bit ADCs," Texas Instruments, Dallas, 2017.

[34] "LPV821, 650nA, Precision, Nanopower, Zero-Drift Amplifier," Texas Instruments, Dallas, 2020.

[35] "MCP4725 12-Bit Digital-to-Analog Converter with EEPROM Memory," Microchip Technology Inc., Chandler, 2009.

[36] "Overview of freshwater quality monitoring and surveillance," Government of Canada, Ottawa, 2017.

[37] "St. Lawrence River: Monitoring Water Quality," [Online]. Available: https://www.canada.ca/en/environment-climate-change/services/st-lawrence-river/water-sediment/monitoring-water-quality.html.

[38] "Power Consumption Benchmarks," Raspberry Pi Dramble, [Online]. Available: https://www.pidramble.com/wiki/benchmarks/power-consumption. [Accessed 6 June 2020].

[39] R. Reese, J. Bruce and B. Jones, Microcontrollers: From Assembly Language to C Using the PIC24 Family, 2nd Edition, Course Technology PTR, 2014.

[40] M. C. Sean McManus, Raspberry Pi For Dummies, For Dummies, 2017.

[41] "Raspberry Pi 3 vs. Raspberry Pi Zero W," Arrow, March 2018. [Online]. Available: https://www.arrow.com/en/research-and-events/articles/raspberry-pi-3-vs-raspberry-pi-zero-w. [Accessed 22 June 2020].

[42] "MCP3424 18-Bit ADC-4 Channel with Programmable Gain Amplifier for Raspberry Pi," Dfrobot, [Online]. Available: https://www.dfrobot.com/product-1182.html. [Accessed 6 June 2020].

[43] "ADS1115 16-Bit ADC - 4 Channel with Programmable Gain Amplifier," Adafruit, [Online]. Available: https://www.adafruit.com/product/1085. [Accessed 6 June 2020].